Title

Search for meteoritic GEMS I: Comparison of amorphous silicates in Paris and Acfer 094 chondrite matrices and in anhydrous chondritic interplanetary dust particles

Authors

Ohtaki, Kenta K

Ishii, Hope A

Bradley, John P

et al.

Publication Date

2021-10-01

DOI

10.1016/j.gca.2021.05.042

Available online at www.sciencedirect.com

ScienceDirect

Geochimica et Cosmochimica Acta 310 (2021) 320–345

Geochimica et Cosmochimica Acta

www.elsevier.com/locate/gca

Search for meteoritic GEMS I: Comparison of amorphous silicates in Paris and Acfer 094 chondrite matrices and in anhydrous chondritic interplanetary dust particles

Kenta K. Ohtaki [a,*], Hope A. Ishii [a], John P. Bradley [a], Krysten L. Villalon [b,c], Andrew M. Davis [b,c,d], Thomas Stephan [b,c], Karen C. Bustillo [e], Jim Ciston [e]

[a] *Advanced Electron Microscopy Center, Hawai'i Institute of Geophysics and Planetology, University of Hawai'i at Mānoa, 1680 East-West Road, Honolulu, Hawai'i 96822, USA*

[b] *Department of Geophysical Sciences, The University of Chicago, Chicago, IL 60637, USA*

[c] *Chicago Center for Cosmochemistry, Chicago, IL, USA*

[d] *Enrico Fermi Institute, The University of Chicago, Chicago, IL 60637, USA*

[e] *National Center for Electron Microscopy, Molecular Foundry, Lawrence Berkeley National Laboratory, Berkeley, CA, USA*

Received 26 October 2020; accepted in revised form 19 May 2021; Available online 27 May 2021

Abstract

Amorphous silicates in meteoritic samples are significant as potential surviving interstellar dust from the formation of the Solar System. Amorphous silicate-rich grains called GEMS, glass with embedded metal and sulfides, are abundant in anhydrous interplanetary dust particles and some ultracarbonaceous Antarctic micrometeorites that have high presolar grain abundances. Some GEMS within these objects have been confirmed to be presolar. GEMS-like material, consisting of amorphous silicate with opaque inclusions, has been identified in the matrices of some primitive meteorites. We use specialized thin specimen preparation and transmission electron microscopy methods to compare the GEMS-like material in Paris (CM) and Acfer 094 (ungrouped) chondrites with GEMS in anhydrous, chondritic interplanetary dust particles. Specifically, we compared the amorphous silicate morphology, degree of partial ordering, elemental composition and dominant iron oxidation state. We find that the amorphous silicates in the GEMS-like materials in Paris and Acfer 094 show incipient ordering and are Fe-rich and highly oxidized, while those in GEMS are fully amorphous, Fe-poor, and anhydrous. From examination of various formation routes for the amorphous silicates, we conclude that the GEMS-like material in Paris and Acfer 094 is not GEMS and that it is unlikely that GEMS-like material accreted as primary amorphous material that retained its original amorphous structure since accretion. We also conclude that the presence of GEMS-like amorphous silicates in chondrite matrix is not a reliable indicator for high degrees of primitivity or pristinity since even mild, complex alteration processes may significantly alter silicate structure. Finally, we propose searches for presolar amorphous silicates in chondrite matrix samples that have been precharacterized by transmission electron microscopy methods to enable direct comparisons of presolar amorphous silicate abundances.

Keywords: GEMS; GEMS-like; Amorphous silicates; Matrix; Paris; Acfer 094; TEM; STEM; EDS; EELS; IDPs

1. INTRODUCTION

Amorphous silicates are among the least-understood solids in extraterrestrial materials despite their potentially

* Corresponding author.
E-mail address: kohtaki@hawaii.edu (K.K. Ohtaki).

https://doi.org/10.1016/j.gca.2021.05.042
0016-7037/

enormous significance. Astronomical observations show that the circumstellar environments around dying stars produce significant quantities of crystalline silicates, ~10–20% (e.g., Kemper et al., 2001; Molster and Waters, 2003), but in the interstellar medium between stars, most of the condensed elements reside within amorphous silicate dust grains (Kemper et al., 2004; Hoppe et al., 2017). Some dust in the interstellar medium retains its isotopic signature from formation around other stars, as presolar circumstellar grains are found in primitive meteorites and must have traveled through the interstellar medium. However, the vast majority of interstellar dust undergoes massive reprocessing, resulting in homogenized isotopic compositions similar to those of the dust that formed in the Solar System (e.g., Zhukovska et al., 2008; Jones et al., 2013). Thus, amorphous silicates observed in primitive meteoritic materials are potentially survivors from the population of interstellar amorphous silicates that dominated the presolar dust from which the Solar System formed. How much of the presolar amorphous silicates from the interstellar medium survive in recognizable form in meteorites remains an open question, since amorphous silicates are, by virtue of their nonequilibrium nature, more susceptible to alteration prior to accretion into, during residence on, and after release from, their parent bodies. Despite their vulnerability to alteration, it has been established that at least some amorphous silicate-dominated grains, observed as rare, sub-μm objects in some interplanetary dust particles (IDPs) and micrometeorites, are unambiguously of presolar origin, because they have nonsolar oxygen isotopic compositions and have not been exposed to postaccretional alteration on their parent bodies (e.g., Messenger et al., 2003). Amorphous silicate-dominated grains with nonsolar oxygen isotopic compositions (e.g., Nguyen et al., 2007) are also found among the rare presolar grains in the fine-grained matrices of some meteorites, although it is less clear if they have preserved their structure since accretion. These nonsolar objects are circumstellar silicate grains that survived, at least in part, their passage through the interstellar medium. A recent estimate of the fraction of surviving interstellar dust incorporated into primitive small solar system bodies is ~5–10% (Alexander et al., 2017) but assumes that interstellar dust has homogenized elemental and isotopic composition. Incomplete processing in the interstellar medium of subcomponents in some dust grains is expected based on the demonstrated survival of presolar silicates. However, these subcomponents may be too small to be detectable among isotopically equilibrated surrounding material. In addition, chemical affinities result in elements combining in preferred ratios with certain other elements. Together, these factors can result in amorphous silicate-dominated grains with sufficient elemental compositional heterogeneity to be nonsolar but without detectable isotope anomalies (Ishii et al., 2018). As such, survival rates of interstellar dust are likely higher than can be determined with current instrument detection limits, and the estimate of Alexander et al. (2017) should be considered a lower limit.

Carbon-rich, anhydrous, chondritic interplanetary dust particles, referred to hereafter as anhydrous IDPs, contain amorphous silicate-dominated grains known as GEMS, where GEMS stands for glass with embedded metal and sulfides (Bradley, 1994; 2014). Anhydrous IDPs have porous and, less-commonly studied, filled morphologies. Ultracarbonaceous Antarctic micrometeorites (UCAMMs) differ in their mode of collection but are similar to anhydrous IDPs in their constituent components, including GEMS (Dobrică et al., 2012; Noguchi et al., 2015). Anhydrous IDPs and UCAMMs contain high abundances of presolar material, where presolar material is identified by its exotic isotopic compositions inherited from its parent star prior to our Solar System's formation. A large portion of this presolar material is silicate-dominated, including both crystalline and amorphous silicates, that are more susceptible to alteration by secondary processing compared to other presolar materials (Floss and Haenecour, 2016). The high abundances of presolar material in anhydrous IDPs and UCAMMs as well as their high porosities and fragile microstructures suggest that they originate from small bodies like comets that accreted at heliocentric distances beyond the giant planets. The uncompacted, porous aggregate structure of anhydrous IDPs and UCAMMs indicates that GEMS grains are primary components that have been preserved since they aggregated into their icy parent bodies. On average, GEMS grains have near-chondritic chemical composition, although individual GEMS compositions vary widely. The amorphous silicate matrix in GEMS grains is highly Mg-rich and Fe-poor and contains embedded inclusions of kamacite and pyrrhotite (Bradley, 1994). GEMS grains are typically embedded in – and admixed at the nanoscale (~10–100 nm) with – low-temperature organic carbon, and the organic carbon surrounding GEMS has been proposed to protect them from the oxidative effects of atmospheric entry (Ishii et al., 2018). The properties of the most pristine GEMS grains reveal that they aggregated in extremely cold environments like the outer nebula, presolar molecular cloud, or interstellar medium (Bradley, 2014 and references therein; Ishii et al., 2018). Their elemental compositions and mineralogical and physical properties are similar to those of silicate dust grains in the interstellar medium (e.g., Bradley, 2014). GEMS have been suggested to have formed as rapidly cooled condensates in the early nebula (Keller and Messenger, 2011) or as radiation-amorphized interstellar silicates (Bradley, 1994). The majority of GEMS grains most likely formed by a combination of processes: extensive irradiation and re-accretion in conjunction with condensation and irradiation of organic carbon precursors during their lifetimes, cycling between diffuse and dense interstellar medium environments and, ultimately, the collapsing presolar molecular cloud (Ishii et al., 2018). At least some GEMS grains are unambiguously of presolar origin or have surviving presolar components as they have nonsolar isotopic compositions (e.g., Messenger et al., 2003; Floss et al., 2006). GEMS grains that are identified as isotopically anomalous are large, most with sizes that fall in the top ~5%, strongly suggesting that instrument detection limits prevent detection of smaller presolar GEMS components due to dilution with surrounding (isotopically normal) material.

GEMS-like material, similar to GEMS in consisting of amorphous silicates with opaque inclusions, has also been

described in the matrices of some meteorites (Greshake, 1997; Leroux et al., 2015; Matsumoto et al., 2019; Nittler et al., 2019; Dobrică and Brearley, 2020). It remains an open, but important, question whether there is a relationship between these GEMS-like materials and GEMS in IDPs. Their amorphous silicate matrix makes GEMS more susceptible to alteration and destruction than presolar grains having crystalline structure and thus a means of constraining conditions experienced during their history. If GEMS grains survived and were incorporated into asteroids and meteorites, then there are implications for grain transport and radial mixing in the solar nebula, the conditions during asteroid accretion, the origin and state of preservation of matrices in primitive chondrites that retain amorphous silicates and, because of the association between GEMS and carbonaceous, the origin of abiotic organic matter in the solar nebula. To address the question as to the relationship between GEMS and GEMS-like materials, we have studied the GEMS-like material in the matrices of two chondrites: Acfer 094, an ungrouped carbonaceous chondrite, and Paris, a CM chondrite, both of petrologic type 2. In both, the presence of amorphous silicate-dominated material in interchondrule matrix (ICM) and fine-grained rims (FGRs) around chondrules has generally been interpreted as an indication of minimal aqueous and/or thermal alteration on their parent bodies (e.g., Greshake, 1997; Hewins et al., 2014).

Acfer 094 is a unique find from the Sahara Desert, a breccia that has similarities to CO and CM chondrites but does not fit into known groups (Newton et al., 1995). While Acfer 094 has high abundances of alteration-prone presolar silicate grains (Nguyen and Zinner, 2004; Vollmer et al., 2009a) and is therefore considered highly pristine, it experienced hot desert weathering and some hydration, and may have also experienced some impact processing (Greshake, 1997; Wasson and Rubin, 2010). The abundant amorphous silicate-dominated material throughout its matrix have been proposed to be circumstellar and/or early nebular condensates (Greshake, 1997; Hopp and Vollmer, 2018). These origins for amorphous silicates require that they have been preserved in the amorphous state in Acfer 094 and other chondrite matrices since their formation by rapid condensation (e.g., Greshake, 1997; Bradley, 1994; Abreu and Brearley, 2010; Palme et al., 2015). Some studies have suggested that the Acfer 094 matrix was unaffected by secondary processes and that the amorphous silicate-dominated material is anhydrous (Newton et al., 1995; Greshake, 1997). Others have considered the possibility that chondrite matrices and the amorphous silicates they contain may be a product of secondary alteration of refractory silicates (e.g., Alexander et al., 1989; Metzler et al., 1992; Howard et al., 2011). Recent reports of a high and homogeneous Fe oxidation state, however, indicate that aqueous alteration on the Acfer 094 parent body led to hydration and oxidation of the amorphous silicate in the meteorite matrix (Hopp and Vollmer, 2018). This interpretation is supported by the observed mobilization of Fe and Ca and the presence of ferrihydrite and nanophyllosilicates, which are few-basal-layer packets of crystallized phyllosilicates forming fibers in the amorphous silicate matrix (Greshake, 1997; Hopp and Vollmer, 2018). Nanophyllosilicate fibers have been interpreted as recrystallization products of hydrated amorphous silicates during early-stage aqueous alteration in Acfer 094 and other chondrites (Hopp and Vollmer, 2018; Chizmadia and Brearley, 2008; Le Guillou et al., 2015). Recent analyses of a high-porosity clast within Acfer 094 matrix proposed its formation by accretion of amorphous silicate grains and primordial ice (Matsumoto et al., 2019).

Paris is a breccia that is considered to be one of the least altered CM chondrites (Hewins et al., 2014). Several microstructural studies of crystalline and amorphous silicates in Paris describe heterogeneity in degree of aqueous alteration and mild thermal metamorphism (e.g., Hewins et al., 2014; Marrocchi et al., 2014; Leroux et al., 2015; Cuvillier et al., 2018; Zanetta et al., 2021). Moderately altered, metal-poor lithologies of subtype 2.7 contain abundant ordered phyllosilicates, whereas minimally altered, metal-rich lithologies of subtype 2.9 $\pm$ 0.1 contain abundant amorphous silicate-dominated material (Hewins et al., 2014; Rubin, 2015). Like Acfer 094, nanophyllosilicates presenting with a fibrous texture have also been observed in Paris, with fewer fibers in amorphous silicate material in the least altered regions and more abundant and coarser fibers in more altered regions. Leroux et al. (2015) observed amorphous silicate grains with inclusions, a few-hundred nm in diameter, of near-chondritic composition, separated by porosity, and with fibrous material in the interstices. They suggested that the amorphous silicate-dominated material is related to GEMS and that "GEMS grains could have been the building blocks of the CM matrices". Leroux et al. (2015) were unable to confirm the mineral identity of Fe-bearing inclusions due to their small sizes. We note that the thickness of FIB sections further complicates identification of Fe-bearing inclusions and assessment of the texture within the amorphous silicate matrix of the GEMS-like material. In somewhat more altered regions, they observed the amorphous silicate as a continuous groundmass containing increased abundance of phyllosilicate fibers and increased overall Fe content, which they attributed to increasing aqueous fluid interaction with the matrix. Recent studies on CM matrices indicate that the Paris meteorite matrix contains ~5–6 wt% H_2O, consistent with other CM falls (Vacher et al., 2020), although Paris is considered a find.

Assessing the origins of amorphous silicates is challenging, since, unlike crystalline silicates, amorphous silicates are metastable. As a consequence, they are highly susceptible to alteration by heating, aqueous processing, and terrestrial contamination. In addition, the amorphous silicate in both IDPs and primitive meteorite matrices contains fine-grained inclusions of other mineral phases. Transmission electron microscopy (TEM) methods are typically employed to characterize the amorphous silicate-dominated GEMS and GEMS-like components in these samples. In many cases, however, inclusions are sufficiently small and well-dispersed throughout the amorphous silicate

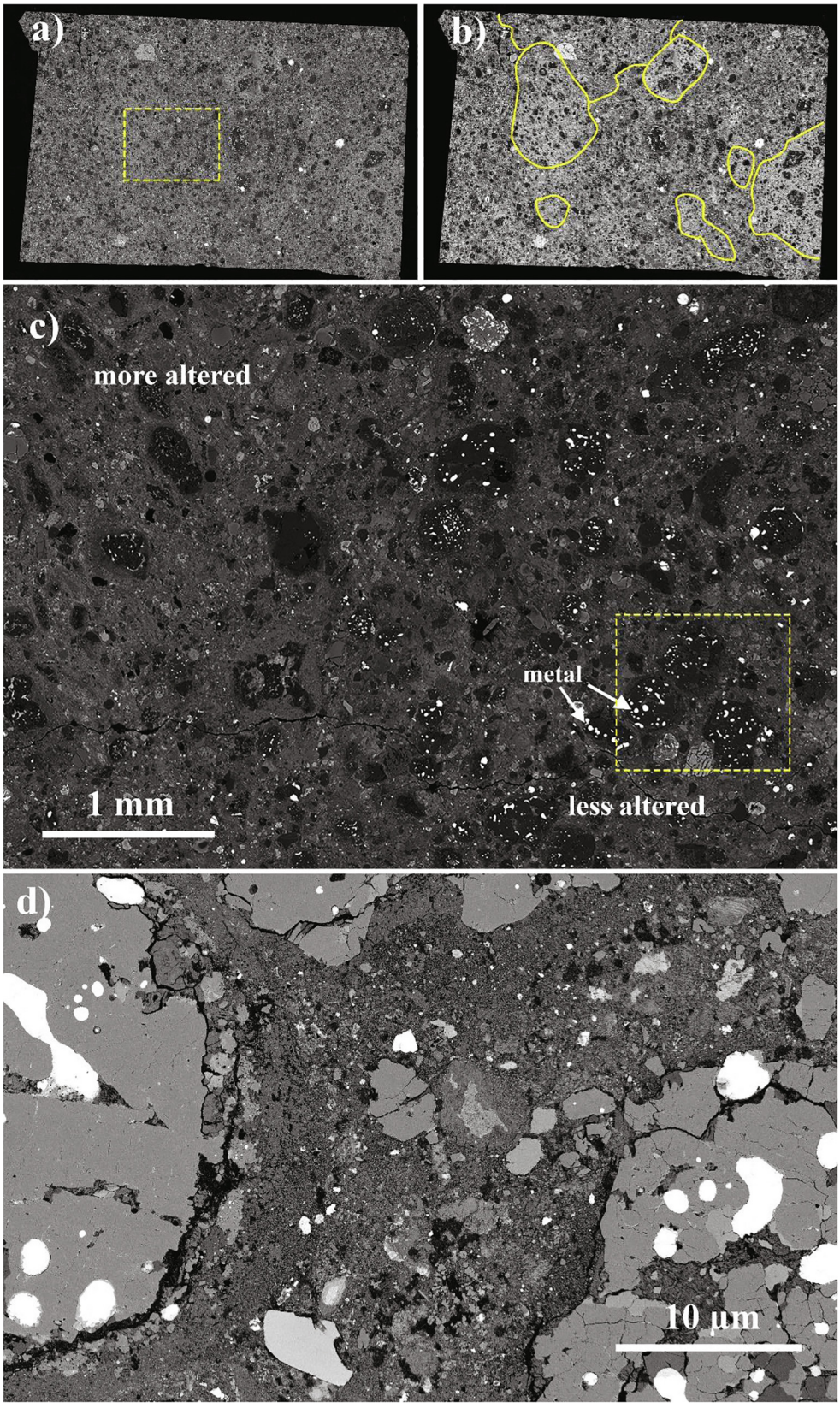
a)
b)
c)
more altered
metal
1 mm
less altered
d)
10 µm

to prevent analysis of the amorphous silicate alone, even using state-of-the-art TEM methods, unless specimens are sufficiently thin (e.g., Brownlee et al., 1999).

In this paper, we apply specialized sample preparation in combination with TEM to exclude mineral inclusions and directly compare the amorphous silicate in the GEMS-like material in the matrix of Acfer 094 and in the matrix and FGRs in the least-altered, metal-rich lithology of Paris with the amorphous silicate within GEMS grains in anhydrous IDPs. The IDPs selected for this study are carbon- and GEMS-rich and show minimal alteration by terrestrial processes. We consider petrographic context, morphology, amorphous silicate elemental composition, Fe oxidation state, and phyllosilicate content in order to assess the likelihood that the GEMS-like material (amorphous silicate with inclusions) in the chondrite matrices is GEMS, was GEMS that was subsequently altered, or has an origin independent of GEMS. This work is complemented by a companion paper by Villalon et al. that compares the inclusions within GEMS-like amorphous silicate-dominated material in Paris to those in GEMS in anhydrous IDPs (Villalon et al., this issue).

2. SAMPLES AND EXPERIMENTAL METHODS

Three GEMS-rich anhydrous IDPs were selected for analysis: U217B19, W7207A, and clast LT29 from U220GCA (referred to as LT29). U217B19 and W7207A were each isolated within a bead of elemental sulfur that was then encapsulated in low-viscosity epoxy. LT29 is a nonporous, compact, red-brown organic carbon clast in a giant cluster particle that was embedded directly in epoxy, but due to its less porous nature, the epoxy (distinguishable by lack of N) did not significantly infiltrate its interior. The embedded IDPs were ultramicrotomed to produce electron-transparent thin specimens, ~40–70 nm in thickness (Bradley and Brownlee, 1986; Bradley, 1994; Keller et al., 2000). These were collected on copper TEM grids with (amorphous) carbon substrates for TEM. The elemental sulfur sublimed away, leaving "naked" particle slices of U217B19 and W7207A on the carbon substrates.

Polished and carbon-coated petrographic sections of Paris (section 2010–7), provided by the Muséum National d'Histoire Naturelle in Paris, and of Acfer 094 (section 094.01) were first surveyed by scanning electron microscopy (SEM). The sections were examined using a JEOL JSM-5900LV SEM instrument equipped with a Thermo Fisher Scientific UltraDry EDS system at the University of Hawai'i at Mānoa (UHM). Backscattered electron (BSE) images and energy dispersive X-ray spectroscopy (EDS) maps were collected at 15 kV. Selected matrix locations were subsequently imaged and mapped at higher resolution, also at 15 kV, using a Helios 660 dual-beam focused ion beam SEM (FIB-SEM, FEI Co., now Thermo Fisher Scientific) instrument equipped with an Oxford Instruments X-MaxN 80 silicon drift detector system at the Advanced Electron Microscopy Center at UHM. Element maps produced by SEM-EDS are shown in 3-color RGB images in which each element is assigned red, green, or blue. EDS data were processed using commercial "remote standards" standardless quantitative analysis software (AZtec Energy Advanced Microanalysis System, Oxford Instruments). Known crystalline silicates (e.g., olivine and pyroxene with a range of compositions) yielded major element abundances within ± 2.5 atomic % of stoichiometry using this approach. Figs. 1 and 2 show BSE images of the chondrite samples prior to sample extractions.

Electron-transparent specimens, also referred to as TEM sections, of Acfer 094 and Paris were prepared using the Helios FIB-SEM and a Leica Ultracut F ultramicrotome. Two methods were employed: a conventional FIB preparation method (e.g., Ishii et al., 2010; Ohtaki et al., 2018; Villalon et al., this issue) and a hybrid FIB-ultramicrotomy method developed specifically for this study of fine-grained matrix that involves extraction of a block of material using FIB methods followed by ultramicrotomy to produce many TEM sections from a single FIB extraction (Ohtaki et al, 2020). Sections prepared using conventional FIB methods are typically 100–150 nm in thickness (e.g., Leroux et al., 2015; Cuvillier et al., 2018; Zanetta et al., 2021; Hopp and Vollmer, 2018). The new combined FIB-ultramicrotomy method enables comparisons of the amorphous silicate components in anhydrous IDPs and meteorite samples by providing thinner meteorite specimens (about 40 nm thick) of the same or similar thickness as the IDP specimens prepared by ultramicrotomy. IDPs are commonly prepared by ultramicrotomy since they are comprised of predominantly sub-μm-sized components that cut well with limited disruption to their original distribution. The thin, ultramicrotomed TEM sections of the amorphous silicate-bearing chondrite matrices allow higher spatial resolution chemical analyses and better avoidance of crystalline inclusions (metal, sulfides, silicates, etc.) that have influenced composition analyses of the amorphous silicate component in the past. Contiguous rocky or glassy phases > 1 μm in size often suffer from blade chatter, brittle fractures created during cutting, that can cause some disruption of the original petrography.

Locations with minimal alteration in the Paris and Acfer 094 samples were selected for TEM sample extraction (Figs. 1 and 2). In the Paris petrographic section, a region that lies between three metal-bearing Type I chondrules in

◀

Fig. 1. Backscattered electron (BSE) images of polished section 2010–7 of the Paris meteorite. (a) Tiled image of the entire section, which is ~2 cm in width. The yellow box indicates the region shown at higher magnification in c. (b) Exaggerated contrast reveals regions of more altered material, outlined in yellow, that appear lighter in contrast overall. (c) Boundary region with metal-poor, more altered lithology in upper left and metal-rich, less altered region in lower right. The yellow box indicates the region shown at higher magnification in d. (d) Region from which samples of fine-grain rim and interchondrule matrix were extracted for TEM analyses. Locations of extracted regions are indicated in Fig. 3b. (For interpretation of the references to colour in this figure legend, the reader is referred to the web version of this article.)

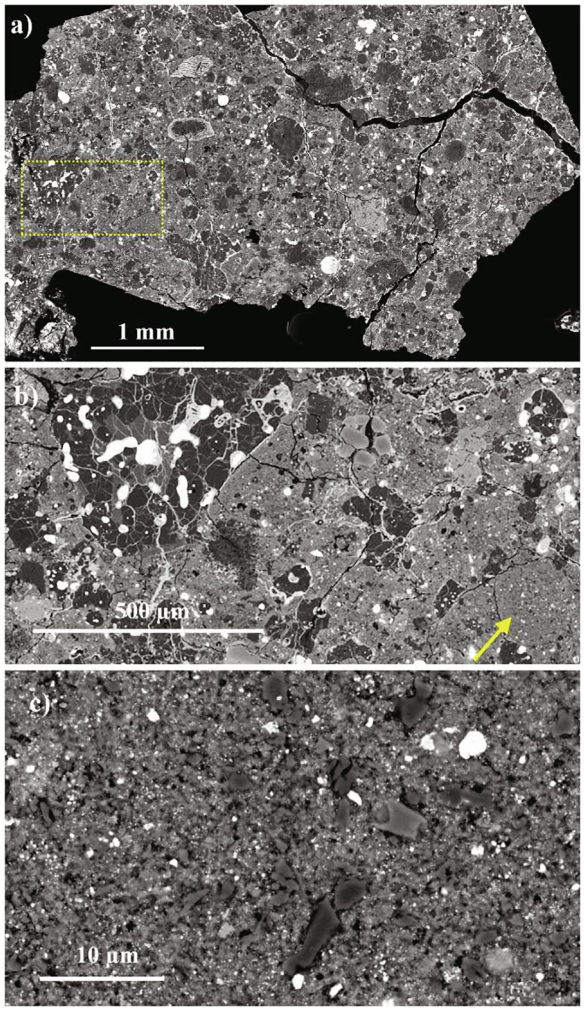

Fig. 2. BSE images of polished section Acfer 094.01. (a) Low magnification image of the majority of the section. The yellow box indicates the region shown at higher magnification in b. (b) Higher magnification image of region from which samples of fine-grained matrix were extracted for TEM analyses. Extraction location is indicated by the yellow arrow. Note the lack of alteration veins nearby this location. (c) Typical morphology of fine-grained matrix in region of extractions. (For interpretation of the references to colour in this figure legend, the reader is referred to the web version of this article.)

the metal-rich lithology was selected for extraction of samples for subsequent TEM/STEM analyses, since the matrix and FGR material within those bounds might reasonably be expected to have experienced minimal alteration on the parent body. Avoiding large crystals and grains, three blocks (~10 × 10 × 8 μm^3) were extracted for ultramicrotomy: one from the interchondrule matrix (ICM), and two from the FGR. The petrographic section of Acfer 094 in this study has cross-cutting Fe-oxide veins that are the result of moderate terrestrial weathering. An ICM-rich region near metal-bearing Type I chondrules and away from weathering veins was selected for extraction for a conventional FIB section and a block for subsequent ultramicrotomy. The selected matrix region is also near a few small, 15–30 µm diameter calcium-aluminum-rich inclusions (CAIs), one with a Wark-Lovering rim (Wark and Lovering, 1977). Extraction locations are shown in detail in the Results section.

TEM sections were prescreened with high-angle annular dark field (HAADF) imaging, EDS, and electron diffraction at 300 kV using a 60–300 kV high-base Titan G2 analytical (scanning) transmission electron microscope (TEM/STEM, FEI Co., now Thermo Fisher Scientific) with a monochromator, dual spherical aberration (C_s) correctors, thin-window energy-dispersive X-ray detector (EDAX), and a high-resolution Tridium electron energy-loss spectrometer (Gatan, Inc.). These initial analyses were used to identify GEMS-like regions containing amorphous silicate matrix with metal-rich inclusions. Additional EDS hyperspectral mapping and electron energy loss spectroscopy (EELS) were performed at the Molecular Foundry, Lawrence Berkeley National Laboratory using a 80–300 kV TitanX "ChemiSTEM" with four windowless X-ray silicon drift detectors (~0.7 sr solid angle, Bruker) and an 80–300 kV high-base Titan G2 STEM with monochromator, chromatic aberration corrector (C_s), dual spherical aberration (C_s) correctors, and a Continuum Model 1069 electron energy-loss spectrometer with a K3 direct electron camera operating in single electron counting mode (Gatan, Inc.), respectively. All samples were monitored for incipient beam damage, and no degradation was observed at the low doses used.

Element compositions reported here were determined from EDS mapping (at the Molecular Foundry). Compositions of amorphous silicate matrix in GEMS and GEMS-like material were determined from EDS hyperspectral maps generated by rastering a sub-nm electron beam with 1.6 or 3.3 nm pixel spacings over regions of ultramicrotomed TEM sections. EDS maps and HAADF images were collected at 200 kV and 500 pA with a detector energy resolution of 140 eV (Mn Kα) and a dispersion of 10 eV/channel for 0–40 keV X-rays. After collection, element distributions were displayed, using the Esprit 1.9 software package (Bruker Corporation), as color-coded maps with the intensity level at each pixel proportional to the integrated counts in an energy window set around characteristic X-ray energies for each element. Element maps generated by TEM-EDS are for visualization only and are not accurate representations of quantitative composition. The Esprit software allows display of more than three elements, and, where multiple elements are overlaid, the colors assigned to each element are not additive. As a result, grayscale images are provided for each individual element in the Electronic Annex. To quantify compositions of amorphous silicates, regions were defined within a given map, excluding any inclusions, and spectra from those regions were summed, background-subtracted, fit, and quantified also using Esprit 1.9 software with remote standardless quantification validated with known composition mineral standards to provide compositions to within ±2% for major elements. Compositions were normalized to 100%. Oxygen abundances should be viewed with caution because oxygen K X-rays are subject to variable amounts of self-absorption by the sample. Three to four maps per

TEM section were collected in order to analyze amorphous silicate compositions and morphologies within the matrix.

Crystalline phases were identified by electron nanodiffraction (at UHM) as appropriate to their small sizes (Bradley, 2019). Nanodiffraction was carried out with an accelerating voltage of 300 kV, camera length of 370 mm, and convergence angle of 0.1–0.3 mrad. Nanodiffraction rings from FIB-deposited nanocrystalline Pt were acquired with the same parameters and used to calibrate d-spacings in reciprocal space.

Oxidation states were measured by EELS using the Continuum spectrometer at the Molecular Foundry. The high signal/noise ratio provided by the K3 camera minimizes electron beam damage to the amorphous silicates and enables rapid mapping of oxidation states at 2–5 nm spatial scales. The 3000 eV wide energy range allows simultaneous recording of the zero loss peak and core loss spectra, eliminating energy drift issues and enabling on-the-fly deconvolution of plural scattering effects. For this study, we used an accelerating voltage of 300 kV, beam current of ~110 pA, a convergence angle of 17.1 mrad, and a spectometer collection angle of 26 mrad. A dispersion of 0.18 eV/channel, 5 mm aperture, and 750 eV slit were used resulting in a measured full width at half max (FWHM) of the zero-loss peak of 0.5 eV.

3. RESULTS

In this section, results of imaging and elemental mapping data obtained using SEM and FIB-SEM over large areas (and at limited spatial resolution) are presented first, followed by imaging, diffraction, elemental mapping, and oxidation state analyses obtained using TEM at finer scales.

3.1. Petrography

The petrographies of the Paris and Acfer 094 chondrites have been described extensively by others (e.g., Newton et al., 1995; Hewins et al., 2014; Zanetta et al., 2021). The local petrography studied by SEM and EDS is described here to provide context for interpretation of data from TEM sections extracted from these samples. The petrography of anhydrous chondritic IDPs has also been well-described in the literature (e.g., Bradley, 2014). The IDPs and their components in this study are too small for SEM-level analysis, but a summary of their overall petrography as observed from TEM sections is provided.

3.1.1. Paris

The region in the Paris chondrite petrographic section selected for TEM studies contains three Type I chondrules as shown in Figs. 3a–f in a BSE image and corresponding 3-color RGB maps of element distributions generated from the EDS mapping. Figs. 3g–l show a higher magnification BSE image of the ICM region from which TEM samples were subsequently extracted and corresponding 3-color element maps with the same element-to-color schemes as in Figs. 3a–f. (See Electronic Annex for individual element maps for each figure.) In the Type I chondrules in this sample, the Mg-rich silicates have compositions of $Fs_{0–3}$ for pyroxene and $Fa_{0–2}$ for olivine. Within these chondrules, kamacite metal is unaltered where fully enclosed by olivine and/or pyroxene and has compositions of 3.9–5.3 at% Ni and trace abundances of P and Cr. The chondrule in the lower left of the Type I chondrule "triad" has retained its round shape, while other chondrules show more advanced alteration. The top chondrule appears in this polished section as separate fragments, with each still retaining unaltered metal. FeO-rich Type II chondrule fragments ($Fa_{31–66}$) are also present (e.g., barred olivine at bottom center in Fig. 3 panels). The Fe-Mg maps in Fig. 3b and h show a gradation between Mg (blue) and Fe (red) signal with more Mg and less Fe near the metal-bearing Type I chondrules. This more Mg-rich region is the FGR. The ICM is the more Fe-rich region between chondrules. Fig. 3h shows patchiness in the Fe content in the ICM from larger Fe-bearing regions. Multiple layers have been observed in FGRs (e.g., Trigo-Rodriguez et al., 2006; Zanetta et al., 2021), and layers with differing BSE contrast (not all continuous) are evident in the BSE imaging of the FGR on the rounded chondrule (Fig. 3g). Two FGR locations were selected next to the rounded Type I chondrule, one (B, inner rim) with brighter BSE contrast and another (A, outer rim) with darker BSE contrast in Fig. 3g. One ICM region (labeled M) was selected near the center of the chondrule triad; these locations are also indicated in Fig. 3. To visualize the distribution of sulfides, Fig. 3c and i include the S signal shown in green, and Fig. 3f and l show Ni, Fe, and S. Discrete coarse-grained sulfides are present in the ICM region, including next to the round chondrule and in the FGR around it. Fig. 3f shows that the sulfides are a mixture of Fe-sulfides and (rarer) Ni-bearing-sulfides (Fe-rich pentlandite with Fe/Ni (atomic ratio) = 0.9–1.8). Fig. 3l shows that Ni-bearing sulfide is present even in the minimally-altered region within the triad of the three metal-bearing chondrules. A mixed silicate and sulfide object (lower left in Figs. 3a–f panels) has alteration products in veins, both Fe- and Ni-bearing-sulfides, and olivine fragments with Mg-rich cores and composition ranges of $Fa_{\sim 10–36}$ that are suggestive of Fe-additive processing. The Fe-S-O maps in Fig. 3d and j show higher average FeO content (purple) in the ICM compared to the FGR and some oxidation around the outer edges of the metal in the Type II chondrules. Figs. 3e and k show altered chondrule mesostasis in the interiors of the chondrules as well as discrete calcium carbonate grains in the ICM. Aluminum and Ca are both present in the ICM and FGR. In Fig. 3j, a large ~50 μm long calcium carbonate grain has a halo of S around it that may be sulfate, since no metal is evident there. These carbonate and sulfur-rich features are present in the minimally-altered region within the triad of metal-bearing chondrules.

3.1.2. Acfer 094

The region in the Acfer 094 chondrite petrographic section from which TEM sections were produced is shown in Figs. 4a–f in a BSE image and corresponding 3-color RGB maps of element distributions generated from the EDS mapping. Fig. 4g shows a higher magnification BSE image of the matrix region from which samples were

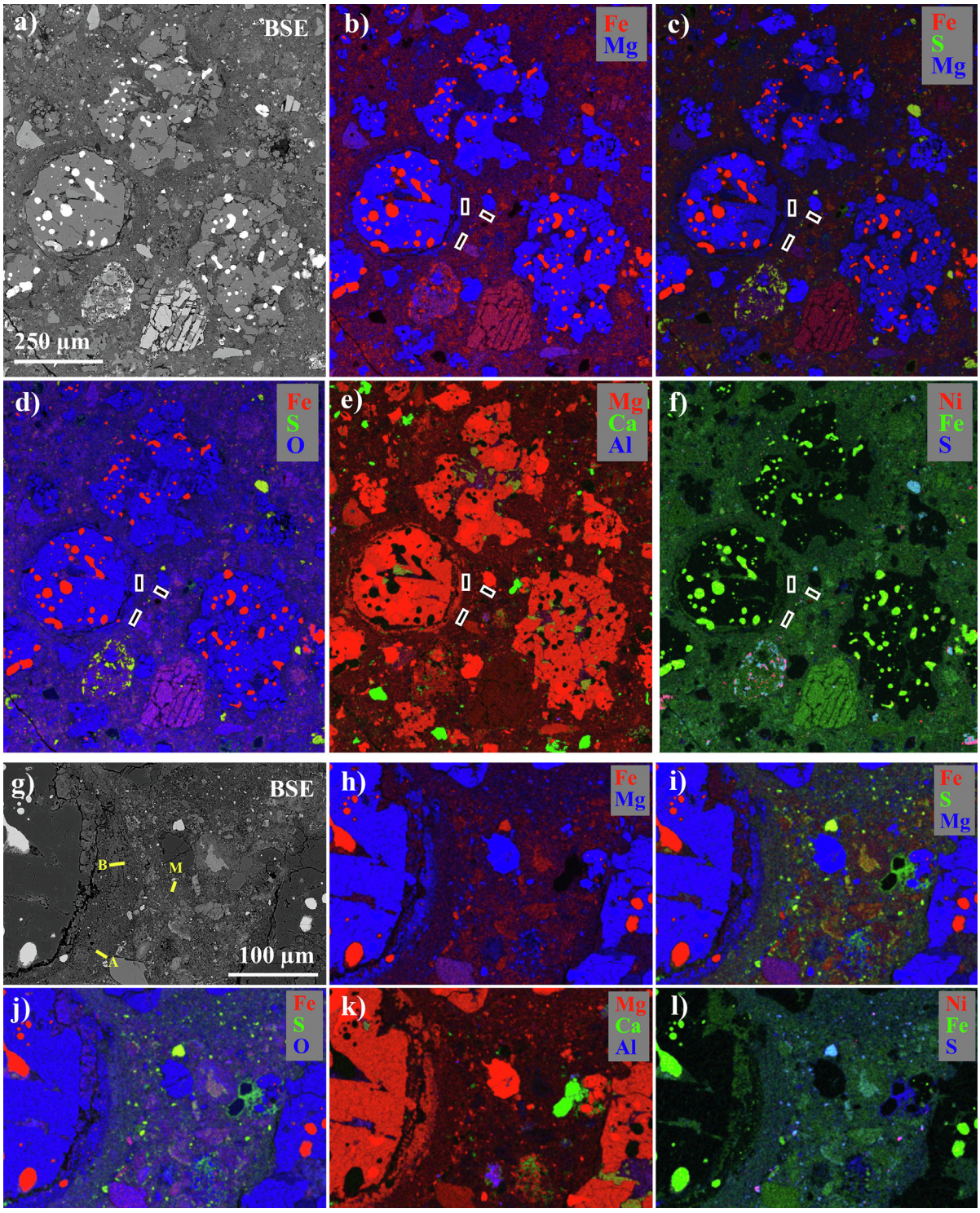

Fig. 3. BSE image collected before, and element maps collected after, sample extractions from a region with three metal-rich chondrules in the Paris chondrite. a) BSE image. The scale bar of 250 µm applies to panels a)-f). b) Element maps of Fe and Mg. White rectangles indicate locations of extraction of blocks for ultramicrotomy. c) Element maps of Fe, S, and Mg. d) Element maps of Fe, S, and O. e) Element maps of Mg, Ca, and Al. f) Element maps of Ni, Fe, and S. g) BSE image of fine-grained rim and interchondrule matrix region in the Paris chondrite prior to extraction. Contrast is enhanced to improve visibility of FGRs. Yellow boxes indicate location and approximate size of extracted blocks for ultramicrotomy. A = FGR-A, B = FGR-B, M = ICM. The scale bar of 100 µm applies to panels g)-l). h) Element maps of Fe and Mg. i) Element maps of Fe, S, and Mg. j) Element maps of Fe, S, and O. k) Element maps of Mg, Ca, and Al. l) Element maps of Ni, Fe, and S.

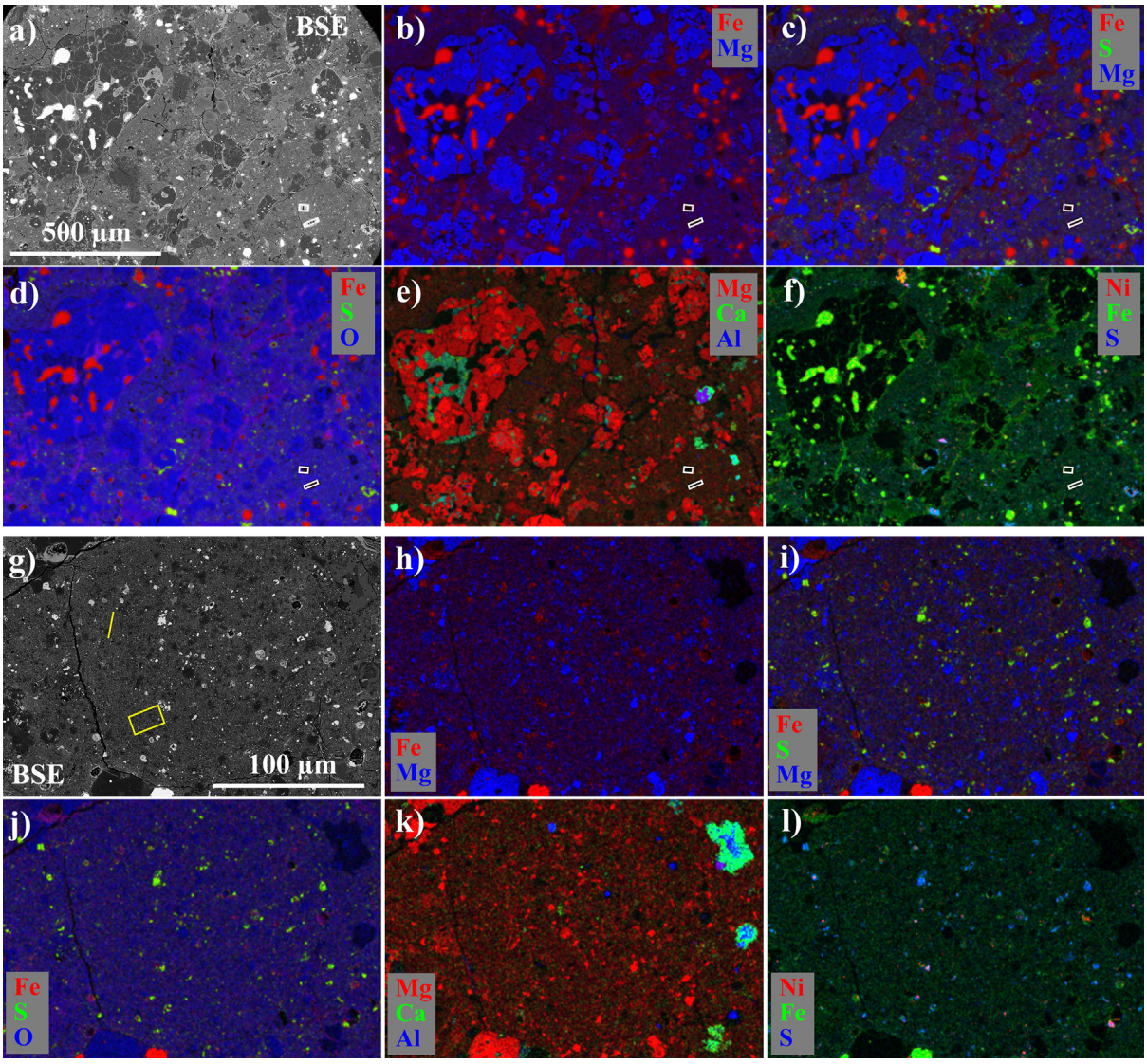

Fig. 4. Image and element maps collected in Acfer 094 prior to extractions. Extraction locations are indicated by white rectangles in each panel. a) BSE image. The scale bar of 500 µm applies to panels a)-f). b) Element maps of Fe and Mg. c) Element maps of Fe, S, and Mg. d) Element maps of Fe, S, and O. e) Element maps of Mg, Ca, and Al. f) Element maps of Ni, Fe, and S. g) BSE image of the site of interest in Acfer 094 prior to extractions. The yellow line and box indicate extraction locations of conventional FIB section and block for ultramicrotomy, respectively. The scale bar of 100 µm applies to panels g)-l). h) Element maps of Fe and Mg. i) Element maps of Fe, S, and Mg. j) Element maps of Fe, S, and O. k) Element maps of Mg, Ca, and Al. l) Element maps of Ni, Fe, and S.

extracted and corresponding 3-color element maps with the same element-to-color schemes as in Fig. 4. (See Electronic Annex for individual element maps for each figure.) In this sample, we observe an extensive network of veins with alteration products due to terrestrial weathering in the Algerian Desert. For example, veins traverse the Type I chondrule in the upper left of the Fig. 4 panels. They are evident in the BSE image in Fig. 4a and the maps that include Fe. Like the Paris Type I chondrules, we find the chondrule olivine and pyroxene to be Mg-rich (semiquantitative composition ranges are $Fa_{0–2}$ and $Fs_{1–3}$) in Acfer 094. The chondrule metal contains ~5 at% Ni and has more extensively oxidized peripheries than in the Paris sample. (See Electronic Annex Fig. S4.) Unlike in the Paris sample, some metal that is not fully oxidized or sulfidized also survived in the ICM. Fig. 4b shows a slight increase in Fe content in the ICM compared to the FGR on the chondrule in the upper left. Acfer 094 is particularly matrix-rich, ~56 vol % (Ebel et al., 2016), and we chose a region of ICM for TEM sample extractions (Fig. 4g) located away from alteration veins that are visible at the surface of the petrographic section. Despite our precautions in site selection, it remains possible that some of the features observed may be products of terrestrial weathering. A few discrete calcium carbonate grains are present in the ICM. In this region, there are also two calcium-aluminum-rich inclusions

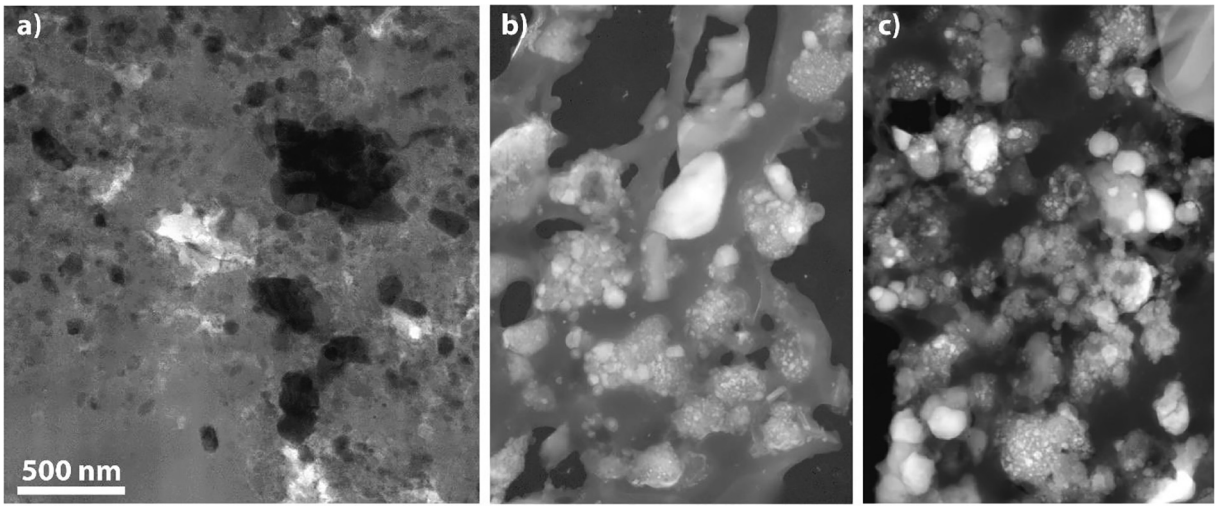

Fig. 5. STEM-HAADF images of amorphous silicate regions in (a) a TEM section of Acfer 094 matrix prepared by conventional FIB extraction and (b) and c) ultramicrotomed TEM sections of IDP U217B19. The darkest areas in the images indicate void spaces. In (a), the middle gray contrast indicates the amorphous silicate regions. The dark gray regions in (b) and (c) are carbonaceous material, and the lighter gray and somewhat-rounded regions containing brighter specks are GEMS having amorphous silicate matrices and inclusions of metal and sulfides. A few crystalline silicates and sulfides are also present. The scale bar of 500 nm in (a) applies to all panels.

(CAIs), about 15 and 30 μm across, evident on the right side of the Mg-Ca-Al map in Fig. 5k by elevated Ca-Al content. Fig. 4d reveals Fe-oxide veins, oxidation of chondrule metal, and higher O content in the ICM surrounding silicate chondrule fragments. Among the chondrule fragments are Type II chondrule fragments of olivine with compositions of $Fa_{20–40}$. Fig. 4c,f and i,l show Fe-S-Mg and Ni-Fe-S maps that reveal the distribution of sulfides. Coarse-grained mixed sulfide-oxide grains are present in the FGR and ICM with a range of compositions that include Fe- and Ni-bearing compositions (atomic Ni/(Fe + Ni) (at. ratio) = 0.1–0.3).

3.1.3. Interplanetary dust particles

The anhydrous chondritic IDPs in this study, U217B19, W7207A, and clast LT29 from U220GCA, contain a high abundance of GEMS (~50% to as much as ~80% of the inorganic components, by area in TEM sections). The GEMS range in diameter from ~50 to 500 nm. Within the amorphous silicate matrix of the GEMS are nanoscale inclusions of Fe,Ni-metal (kamacite) and low-Ni, Fe,Ni-sulfides (pyrrhotite). Crystalline phases are sub-μm pyrrhotite and occasional anhydrous silicate crystals up to a few μm in size. The silicates are enstatite and forsterite (Mg# >95). In contrast to the chondrite matrices, there is no evidence of aqueous alteration: The phases present are unequilibrated, and there are no phyllosilicates, carbonates, or pentlandite present. Organic material forms a porous matrix that binds the GEMS and crystalline components together. Figs. 5b,c and 6a–d show images from typical TEM sections from these IDPs.

3.2. Morphology of GEMS and GEMS-like material

Dark field (HAADF) imaging and EDS hyperspectral mapping were used to investigate the TEM-scale morphology and elemental chemistry of the GEMS-like material in Paris and Acfer 094 chondrites and of GEMS in the IDPs. GEMS-like material was found in both ultramicrotomed and conventional FIB-prepared TEM sections from the chondrite samples, demonstrating that the amorphous silicate is indigenous and not generated by ion beam damage. HAADF images of a conventional FIB-prepared TEM section of Acfer 094 matrix and of ultramicrotomed TEM sections of IDPs are compared in Fig. 5. The conventional FIB section allows comparison of the shapes and sizes of amorphous silicate-rich regions in Acfer 094, undisturbed by ultramicrotome blade chatter. Although conventional FIB sections were prepared from Paris, they were not extracted from the minimally altered 3-chondrule region and may represent more altered matrix, so we refer to the FIB sections prepared from minimally altered Paris matrix by Leroux et al. (2015) and by Villalon et al. (this issue) in our later discussion. The IDPs studied are sufficiently fine-grained that their GEMS sliced cleanly without fracturing, or "chattering", in ultramicrotomy. HAADF imaging with EDS hyperspectral mapping was also performed on ultramicrotomed sections of all samples, Paris FGRs, Paris ICM, Acfer 094 ICM, and GEMS in IDPs, and are compared in Fig. 6. (See Electronic Annex for individual element maps for Fig. 6.)

HAADF images and EDS hyperspectral mapping in Fig. 5b,c and 6a–d show that GEMS grains in the IDPs generally occur as discrete partially rounded objects or agglomerates, several tens to a few hundreds of nm across, often separated by organic carbon. The GEMS-like material in the Acfer 094 ICM, in contrast, forms a contiguous mass with rounded void spaces interspersed over multi-μm-sized scales (Fig. 5a). Blade chatter from the ultramicrotomy process is evident in the presence of fragments with fractured edges having a preferred orientation in the Paris and Acfer 094 samples in Fig. 6. The element maps generated by EDS show that the

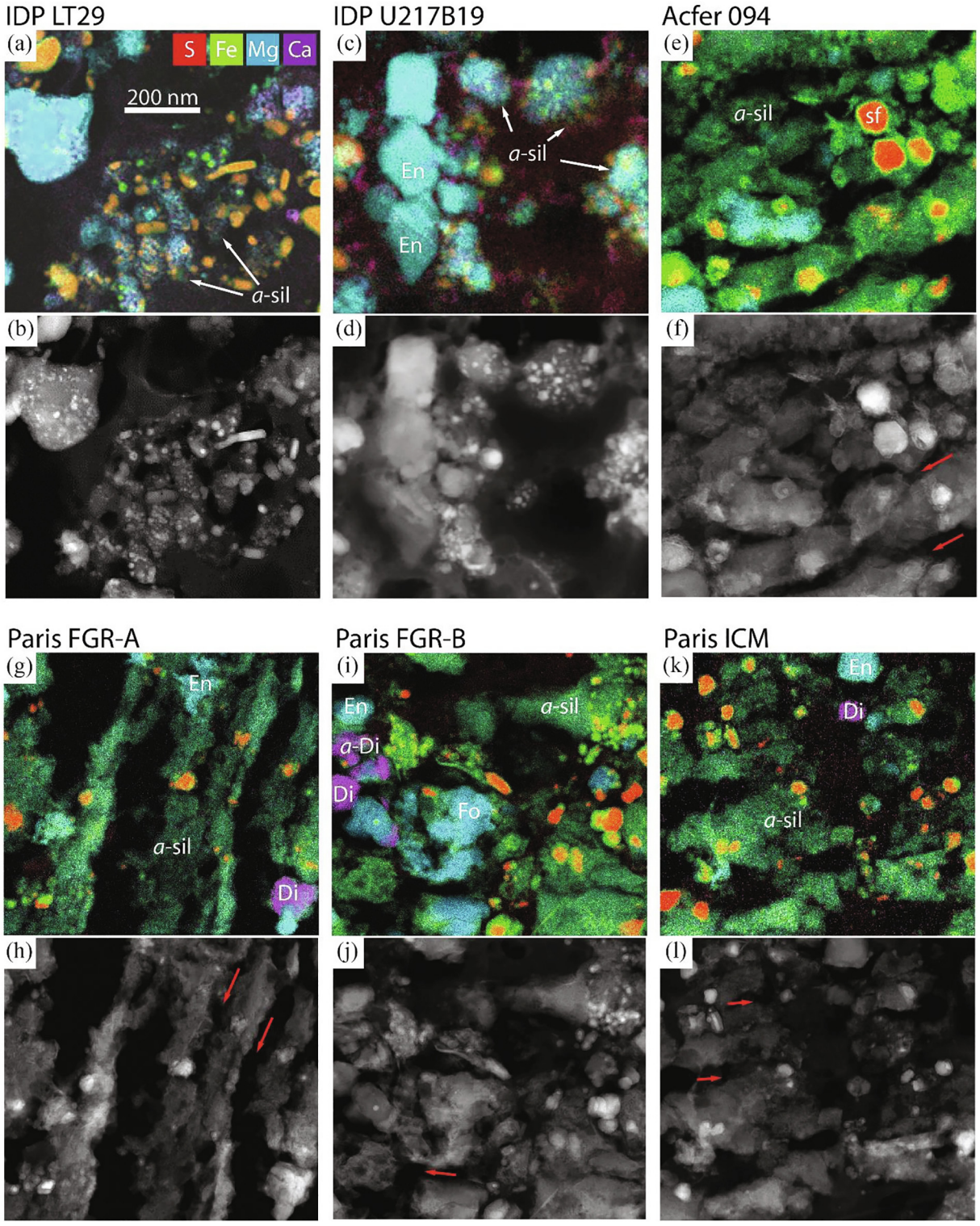

Fig. 6. Representative overlaid EDS maps (top) and STEM-HAADF image (bottom) of ultramicrotomed sections of (a and b) IDP LT29, (c and d) IDP U217B19, (e and f) Acfer 094 ICM, (g and h) Paris FGR-A (outer rim) (i and j) Paris FGR-B (inner rim) and (k and l) Paris ICM. Blue = Mg, red = S, purple = Ca, and green = Fe. Fo = forsterite, En = enstatite, Di = diopside, a-sil = amorphous silicate, a-Di = amorphous silicate with diopside composition, sf = sulfide. Note that, unlike in Figs. 3 and 4, colors are not additive in these TEM-EDS maps. Sulfides appear orange, and metal and metal-oxide appear green. Red arrows in panels f, h, j and l indicate approximate orientation of fractures caused by ultramicrotome blade chatter. See Electronic Annex for grayscale images of individual elements. The scale bar of 200 nm in a) applies to all panels.

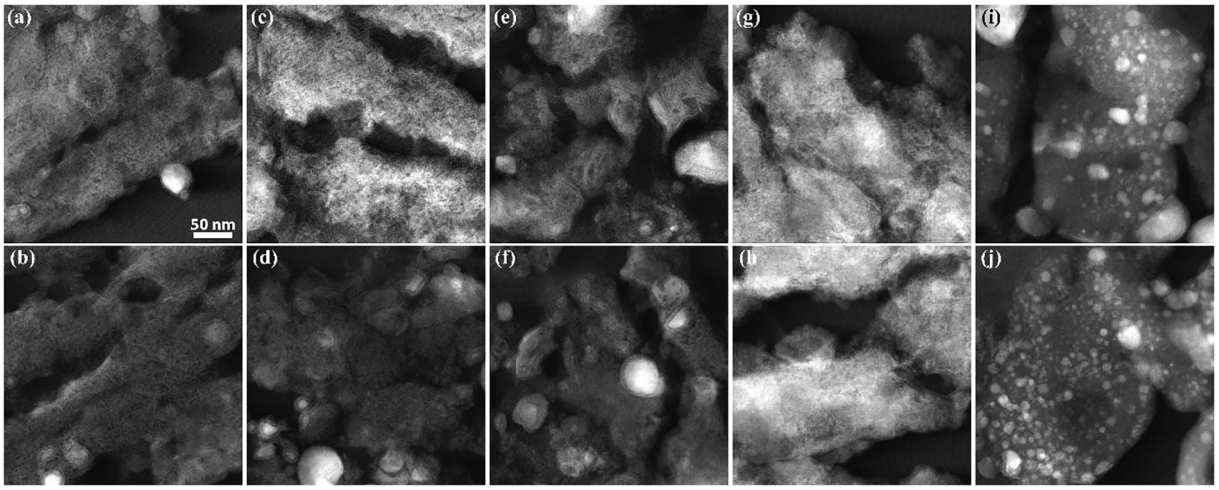

Fig. 7. HAADF images of amorphous silicate in (a) and (b) Paris FGR-A (outer rim), (c) and (d) Paris FGR-B (inner rim), (e) and (f) Paris ICM, (g) and (h) Acfer 094 ICM, and (i) and (j) IDP LT29. The scale bar of 50 nm in a) applies to all panels.

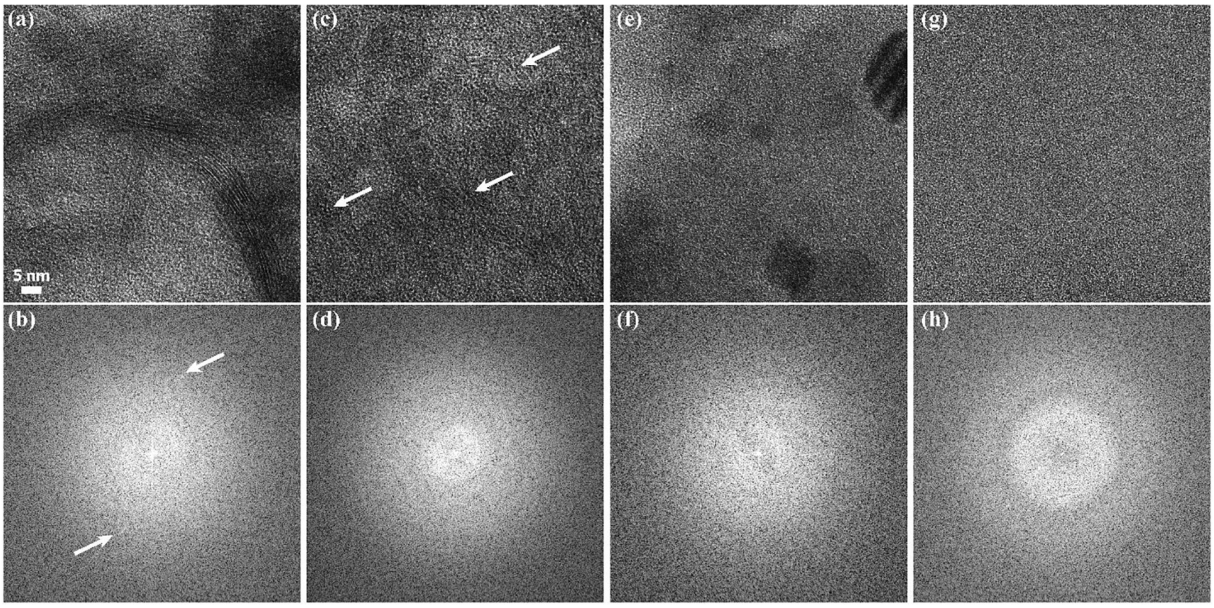

Fig. 8. HRTEM images of amorphous silicate matrix and their corresponding fast Fourier transforms (FFTs) from (a and b) more altered region in Paris with multilayer packets of phyllosilicates, (c and d) less altered region in Paris with shorter fibers of nanophyllosilicates, (e and f) amorphous silicate matrix in GEMS (dark inclusions are metal and sulfide), and (g and h) an amorphous carbon film substrate. Scale bar of 10 nm applies to all upper panels in this figure. The phyllosilicate in (a) has basal spacing of ~0.72–0.73 nm consistent with serpentine. The FFTs in the lower panels all show diffuse rings consistent with amorphous structure. The FFT in (b) has streaks, indicated by arrows, corresponding to (curved) phyllosilicate crystals present in the corresponding image (a).

amorphous silicate matrix of GEMS in IDPs has significantly lower Fe content than that of the GEMS-like material in Paris or Acfer 094 (see Section 3.4 below).

Also, readily apparent from the mapping is that inclusions are significantly smaller in size in the GEMS in IDPs (Fig. 6a–d) than in the chondrite matrices (Fig. 6e–l). In the GEMS in IDPs in this study, metal inclusions have diameters of ~2–10 nm, and sulfide inclusions have diameters of ~5–25 nm. A detailed study of the inclusions in the GEMS-like material in the ICM and FGRs of Paris is provided by Villalon et al. (this issue), a companion paper to this work. We recount here some details obtained from EDS mapping that are relevant to interpretation of the origin of the GEMS-like material in Paris matrix: sulfide

grains are ~10–100 nm in diameter and a mix of pyrrhotite and pentlandite, and Fe-metal grains are smaller, ~10–30 nm, with oxide rims and are associated with sulfide. We note that some metal is within sulfide grains (e.g., Villalon et al., this issue). In the outer FGR, we found a region of amorphous silicate, lacking inclusions and identified by nanodiffraction (Electronic Annex Fig. S12), with a diopside composition identical to crystalline diopside found in the inner FGR and ICM. We also observe that the crystalline silicate grains are not highly faceted, and many show roughened surfaces, indicative of *in situ* alteration at their perimeters. In the set of Paris TEM samples analyzed here, Fe-deficient, Ni-rich sulfides were observed in the ICM but not in the FGRs. Forsterite, enstatite, pyrrhotite, and pentlandite have been identified in the GEMS-like material in Acfer 094 ICM by Greshake, 1997 and, more recently, by Matsumoto et al. (2019). For comparison, the inclusions in the IDP GEMS are Fe-metal (kamacite) and pyrrhotite; pentlandite is not found in the IDP GEMS.

3.3. Order/disorder in amorphous silicates in GEMS and GEMS-like material

High-resolution lattice-fringe imaging and electron nanodiffraction patterns collected at 300 kV were used to investigate the texture and structure of the amorphous silicate-bearing regions. Electron diffraction patterns collected in the back focal plane have diffuse rings indicating presence of amorphous structure in GEMS-like regions in the Paris and Acfer 094 chondrite samples, but because electron beam damage can rapidly amorphize beam-sensitive phyllosilicates at the doses required to collect a diffraction pattern, Fast Fourier transforms (FFTs) of high-resolution images were employed to explore structure. HAADF images in Fig. 7 show that the GEMS-like material in both meteorite matrices exhibit fibrous textures, the extent of which varies across the Paris samples (Fig. 7a–h). The GEMS-like regions in Paris FGRs and in Acfer 094 ICM have a fine fibrous texture, whereas those in Paris ICM have larger, more ordered regions of fibers. Lattice-fringe imaging confirms the fibrous texture is due to packets of ordered phyllosilicates (nanophyllosilicates) with basal spacings of 0.7–1.2 nm (Fig. 8a, c, and e). The conventional FIB section of Acfer 094 ICM shows some variation in the amount of fine fibrous material, with less in the regions that appear smoother than in regions with more void spaces in the HAADF image in Fig. 5a. The amorphous silicates within GEMS, on the other hand, are featureless and devoid of evidence of any ordering in the HAADF images (Fig. 7i–j, and 8e). These subtle textural and structural differences between the amorphous silicates in GEMS and those in the GEMS-like material in chondrite matrices are also evident in diffraction patterns produced from FFTs of the images (Fig. 8b, d, and f). For comparison, a lattice-fringe image of an amorphous carbon support film and its corresponding FFT are shown in Fig. 8g and h. The lower scattering power of the carbon support film results in a negligible contribution to the diffraction patterns from the silicate-dominated materials.

3.4. Elemental compositions of amorphous silicate in GEMS and GEMS-like material

The average major element compositions of the amorphous silicate in the GEMS-like material in Paris and Acfer 094 meteorite matrices and in GEMS from IDPs, all obtained by EDS hyperspectral mapping of ~40 nm thick ultramicrotomed sections, are shown in Table 1, expressed as atomic ratios relative to Si. See Electronic Annex for individual analyses. Individual analyses are plotted on ternary diagrams in Fig. 9.

From the Mg-Si-Fe ternary diagrams in Fig. 9a–c and Table 1, we find that the Fe content in amorphous silicate in Paris GEMS-like material in our samples typically falls between 15 and 40 at% with average Fe/Si of ~0.45–0.60. The Fe content is slightly higher in the Paris outer FGR than the inner FGR or ICM in the 3-chondrule region we sampled in the metal-rich lithology. Mg ranges from ~15 to 30 at% with average Mg/Si of ~0.40–0.50. The Paris compositions are centered at ~20 at% Mg, ~55 at% Si, ~25 at% Fe. In amorphous silicates in Acfer 094 GEMS-like material, Fe contents typically falls between 20 and 55 at% with average Fe/Si of 0.69, Mg content falls between 10 and 25 at% with average Mg/Si of 0.32, and the compositions are centered near ~15 at% Mg, ~50 at% Si, ~35 at% Fe. Although the fields of composition for Paris and Acfer 094 amorphous silicates have some overlap, Acfer 094 tends to be more Fe-rich. Table 1 also shows that the standard deviations of the mean Fe/Si and Mg/Si values in Acfer 094 are larger than in Paris, indicating more variability in compositions in Acfer 094 and not reflecting a difference in measurement uncertainties.

The range of Fe content in the amorphous silicate of GEMS from IDPs is notably lower, between 0 and ~10 at % with an average Fe/Si of 0.15, than in amorphous silicates from both chondrites (Fig. 9 and Table 1). The typical range of Mg content in the amorphous silicate of GEMS, ~10–60 at%, is much wider than in either of the chondrites, with an average Mg/Si of 0.87. As shown in Table 1, the standard deviation of the means of the element/Si ratios is much larger in the amorphous silicates in GEMS and in bulk GEMS with inclusions than in the amorphous silicates in GEMS-like material in the chondrite samples, indicating the wide range of compositions.

Although the Mg-Si-Fe composition of the amorphous silicates in Paris GEMS-like material is more uniform than those in Acfer 094 or in IDP GEMS, small local variations between the ICM and FGRs are evident as shown in Fig. 9a. The Paris FGR-B (inner rim) has slightly more Fe and less Si than FGR-A (outer rim), and the ICM composition has the lowest Fe content. The differences are small, however, and the Paris composition fields for ICM, FGR-A, and FGR-B overlap. Prior analyses by Leroux et al. (2015) on (thicker) conventional FIB-prepared TEM sections, also shown in Fig. 9a, have slightly lower Si and greater range in Fe content than our analyses on ultramicrotomed TEM sections. The prior analyses on (thicker) FIB sections of Acfer 094 GEMS-like material by Hopp and Vollmer (2018) show lower Mg content and extend to higher Fe content than our analyses, as shown in Fig. 9b.

Table 1
Average composition, from EDS mapping in a TEM, given as element/silicon atomic ratios, of amorphous silicate regions in Paris ICM, Paris FGR-A (outer rim), Paris FGR-B (inner rim), Acfer 094 ICM and GEMS; bulk GEMS with inclusions; and solar abundances derived from CI chondrites. Uncertainties are given as 1σ standard deviations. The large standard deviations for GEMS amorphous silicate and bulk GEMS compositions reflect the high intrinsic variability in their compositions.

Average compositions	Mg/Si	Al/Si	S/Si	Ca/Si	Fe/Si	Ni/Si
Paris ICM amorphous silicates, N = 39	0.40 ± 0.10	0.12 ± 0.02	0.03 ± 0.01	0.00 ± 0.00	0.45 ± 0.10	0.02 ± 0.01
Paris FGR-A amorphous silicates, N = 26	0.39 ± 0.06	0.10 ± 0.01	0.02 ± 0.01	0.01 ± 0.00	0.49 ± 0.07	0.03 ± 0.01
Paris FGR-B amorphous silicates, N = 40	0.48 ± 0.08	0.13 ± 0.02	0.05 ± 0.02	0.00 ± 0.00	0.61 ± 0.13	0.03 ± 0.01
Acfer 094 ICM amorphous silicates, N = 54	0.32 ± 0.16	0.09 ± 0.02	0.03 ± 0.02	0.04 ± 0.01	0.69 ± 0.33	0.04 ± 0.02
GEMS amorphous silicates, N = 60	0.91 ± 0.36	0.08 ± 0.03	0.09 ± 0.11	0.03 ± 0.02	0.15 ± 0.12	0.01 ± 0.01
Bulk GEMS, with inclusions, N = 193	0.61 ± 0.28	0.10 ± 0.04	0.25 ± 0.20	0.04 ± 0.04	0.43 ± 0.30	0.03 ± 0.03
Solar abundances (CI)*	1.03	0.08	0.44	0.06	0.88	0.05

* From Table 3 in Palme et al. (2014).

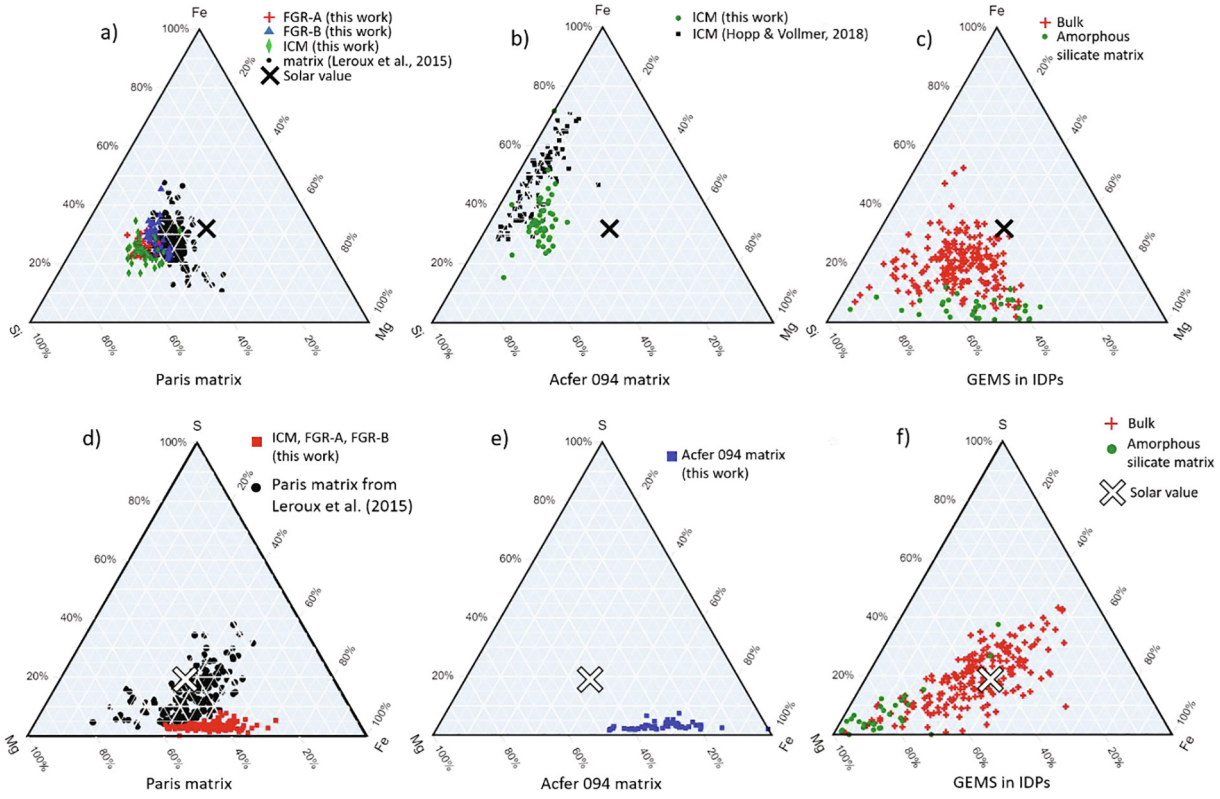

Fig. 9. Ternary plots of elemental composition in amorphous silicate regions: (Top row) Ternary plots of Mg-Si-Fe (atom %) in (a) amorphous silicate regions in Paris FGR-A (outer rim), FGR-B (inner rim), and ICM analyzed in this work and in previous work by Leroux et al. (2015), (b) amorphous silicate regions in Acfer 094 ICM analyzed in this work and in previous work by Hopp and Vollmer (2018), and (c) amorphous silicate in GEMS, avoiding nanoscale inclusions, as well as bulk GEMS that include inclusions. (Bottom row) Ternary plots of Fe-Mg-S (atom %) in (d) amorphous silicate regions in Paris ICM and in Paris FGRs analyzed in this work and in previous work by Leroux et al. (2015), (e) amorphous silicate regions in Acfer 094 ICM analyzed in this work, and (f) amorphous silicate in GEMS, avoiding nanoscale inclusions where they are detected, and bulk GEMS that include inclusions. Solar values are from Palme et al. (2014). (Color images are available online.)

Fe-Mg-S compositions of amorphous silicates in GEMS and GEMS-like material are plotted in Fig. 9d–f. The amorphous silicates in all samples are low in S, confirming that sulfide inclusions have been largely avoided in the present analyses. Compositions of bulk GEMS, including their Fe metal and sulfide inclusions, cluster near solar values and overlap with the Paris ICM analyses of Leroux et al. (2015).

3.5. Oxidation states of iron in amorphous silicate in GEMS and GEMS-like material

The oxidation states of Fe in the amorphous silicate matrices of GEMS-like material in Paris and Acfer 094 were measured and compared using EELS. Fig. 10 contains spectra with Fe-$L_{2,3}$ core scattering edges collected from specific areas in the TEM samples. The dominant oxidation

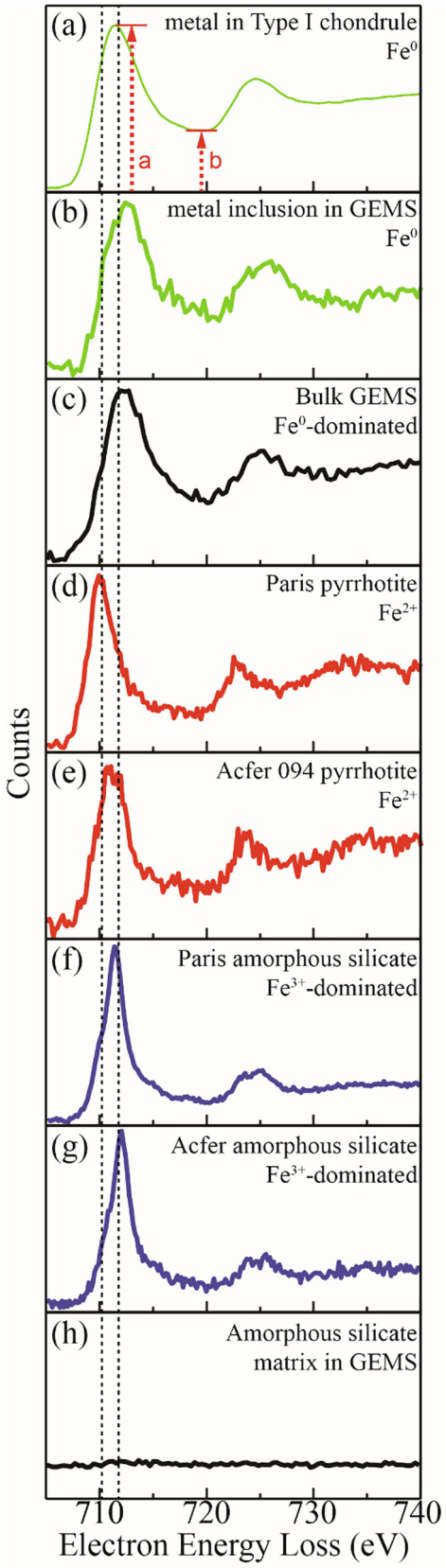

state is distinguished by the chemical shift and core–edge jump ratio (a/b) on the Fe-$L_{2,3}$ core scattering edges (Jin et al., 2006; Tan et al., 2012). Assuming minimal plural scattering, Fe^0 exhibits the lowest pre- to post-edge jump ratio. Fe^{2+} and Fe^{3+} both exhibit higher jump ratios and ~1.8 eV in chemical shift between them. Large metal (>1 μm) (kamacite, $(Fe,Ni)^0$) and pyrrhotite (~$(Fe,Ni)^{2+}S$) grains were identified by elemental chemistry, confirmed by electron nanodiffraction and used for *in situ* oxidation state evaluation. Metal grains from Paris and an IDP give spectra for the Fe^0 oxidation state (Fig. 10a and b), and the Paris and Acfer 094 pyrrhotite spectra are consistent with Fe^{2+} oxidation state (Fig. 10d and e). The spectra from amorphous silicates in GEMS-like material in both the Paris and Acfer 094 matrices are dominated by Fe^{3+} (Fig. 10f and g). Due to near-zero Fe content, there is insufficient signal to observe the Fe core scattering edge in the amorphous silicate in GEMS (Fig. 10h). EELS from bulk GEMS shows that Fe is present predominantly in the Fe^0 state (Fig. 10c), although sulfides were present in the analysis volume, and spectra from individual sulfide inclusions show the Fe^{2+} state.

3.6. Carbon association with amorphous silicates

All IDPs in this study contain occasional μm-scale Mg-rich crystalline silicates, abundant amorphous silicate-dominated GEMS grains, and abundant organic carbon. Carbonaceous material can be seen surrounding and binding GEMS grains together in the HAADF imaging of GEMS-rich IDPs (Fig. 5b and c) and in C element maps extracted from EDS hyperspectral maps in Fig. 11. The GEMS in the IDP TEM sections were not directly exposed to the epoxy embedding medium during preparation but are mounted on amorphous carbon substrates. Since the carbon substrates are thin and uniform, the C maps provide an illustration of carbon's close association with GEMS and its high abundance above the carbon substrate background. (Careful background subtraction can be performed to extract quantitative C abundances, e.g., Ishii et al., 2018). The (porous) chondrite matrix samples in this study were epoxy-embedded during petrographic section preparation in addition to TEM sections being mounted on amorphous carbon substrates. As a result of epoxy infiltration, the distributions of intrinsic carbon in the chondrite samples are obscured by epoxy contamination, so direct comparisons of carbon abundance between GEMS in IDPs and the chondrite matrices are not possible.

Fig. 10. Electron energy loss spectra, integrated over regions of interest, of Fe-$L_{2,3}$ core scattering edges from (a) metal in a Type I chondrule in Paris, (b) a metallic Fe inclusion in an IDP, (c) whole GEMS, including metallic Fe and sulfide inclusions, (d) Fe-sulfide inclusion in Paris, (e) Fe-sulfide in Acfer 094, (f) amorphous silicate in Paris matrix, (g) amorphous silicate in Acfer 094 matrix and (h) amorphous silicate in IDP GEMS. The pre- to post-edge jump ratio (a/b), illustrated in (a)), and the chemical shift in the absorption edge (illustrated by the vertical lines) can be used to distinguish the dominant oxidation state of Fe.

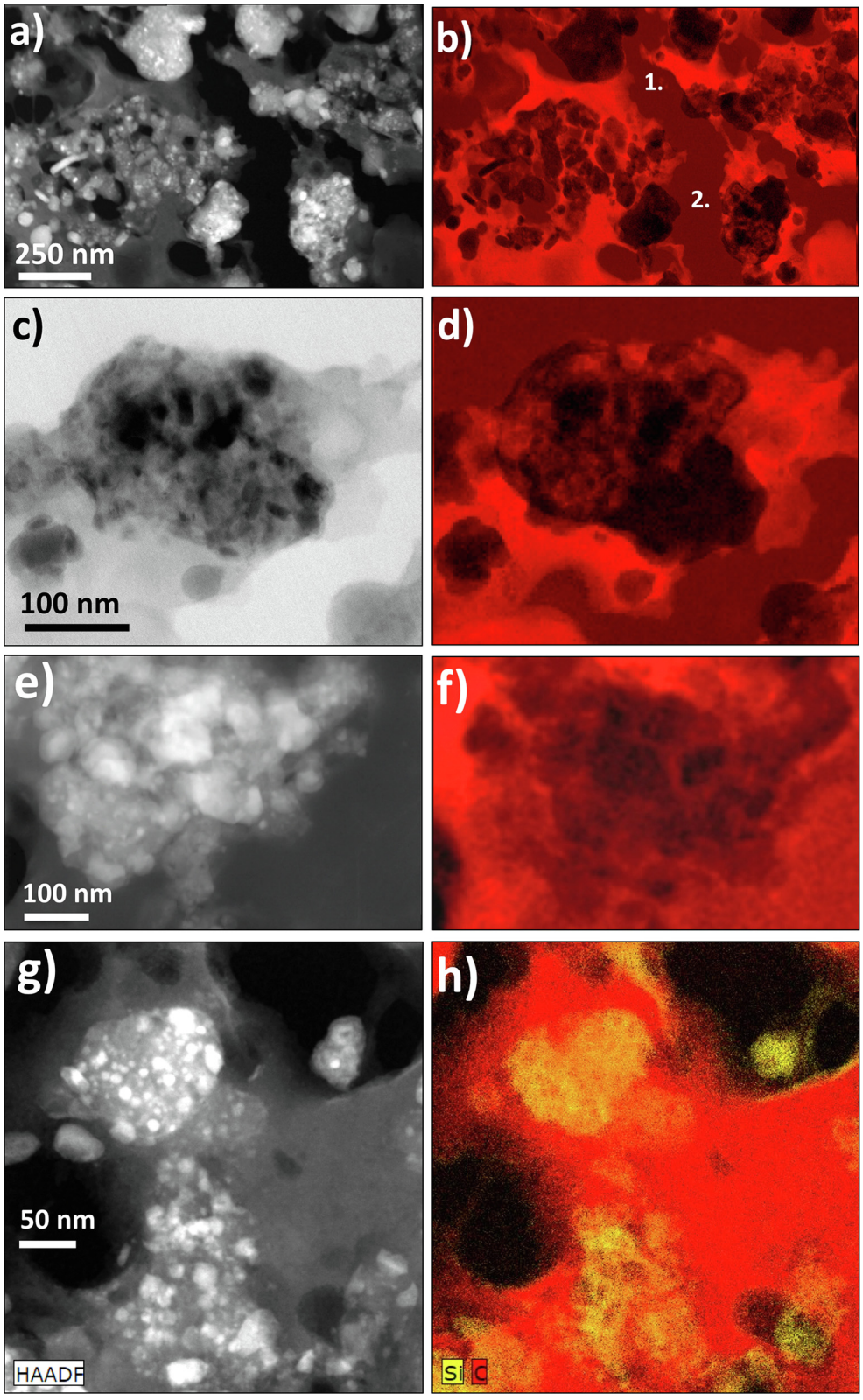

Fig. 11. Petrographic relationship between amorphous silicates (GEMS) and organic carbon in IDPs. Darkfield (HAADF) images (left) and compositional maps (right) for GEMS in (a and b, c and d, g and h) LT 29 and (e and f) U217B19. Red = C, yellow = Si. The carbon substrate (labeled 1 and 2) appears as dark red in some compositional maps. (For interpretation of the references to colour in this figure legend, the reader is referred to the web version of this article.) (Color images are available online.)

4. DISCUSSION

In this section, we discuss first the significance of thin specimens for comparing amorphous silicate compositions without contamination by inclusions. Then, we consider whether the GEMS-like material in Paris and Acfer 094 chondrites is comprised of GEMS and assess other possible origins. It is worth noting here that the term "minimally altered" has different meanings to the IDP and primitive chondrite research communities. Relative to the least-altered IDPs, even the least-altered chondrites have experienced significant secondary alteration on their parent bodies. Paris and Acfer 094 are partially hydrated and fairly strong, well-formed rocks, whereas IDPs are anhydrous, uncompacted aggregates with little or no mechanical strength that readily disaggregate. As evidenced by their fully amorphous structure, anhydrous state, and uncompacted environment, the amorphous silicates in GEMS grains within IDPs were clearly far less altered by parent-body processes. IDPs experience alteration by heating and oxidation during atmospheric entry, and their small sizes and high porosities render them susceptible to subsequent contamination and leaching (e.g., Bradley, 2014, and references therein). Nonetheless, well-preserved GEMS are distinguishable from altered GEMS by chemical and morphological changes. Uncertainties about parent-body alteration of meteorites and terrestrial alteration of IDPs are major contributors to ongoing questions about the origins and significance of amorphous silicates in primitive meteoritic materials. The discussion below is written from the perspective of the IDP concept of minimal alteration.

4.1. Impact of ultrathin TEM sections on composition analyses

TEM section thickness is an important factor in enabling assessment of the true composition of amorphous silicate when fine-grained inclusions are present. Prior analyses of GEMS-like material in the matrices of Paris and Acfer 094 (Leroux et al., 2015; Hopp and Vollmer, 2018) were carried out on conventional FIB-prepared TEM sections, and both studies reported Fe content in amorphous silicate matrix in GEMS-like material extending more frequently to higher values than observed in this work, as evident in Fig. 9a and b. Leroux et al. (2015) also measured significant S content in the amorphous silicate in GEMS-like material in Paris, whereas the present study found very little S in the amorphous silicate (Fig. 9d). These differences are most likely due to the challenges of excluding fine-grained Fe-bearing inclusions (primarily sulfides) in thicker FIB sections, which are typically ~100–150 nm and usually thicker than the ~40 nm thick ultramicrotomed sections produced by the hybrid FIB-ultramicrotomy method used here (Ohtaki et al., 2020). The relatively "large" inclusions in the Paris GEMS-like material compared to those in GEMS in IDPs (Villalon et al., this issue) are readily excluded in composition analyses from our high spatial resolution EDS hyperspectral mapping of ultramicrotomed sections. We observe Fe,Ni-metal nanocrystals in the amorphous silicate matrices of some GEMS in IDPs down to diameters of 1–2 nm that are especially challenging to observe and exclude from EDS maps since they approach the single pixel size, even with ultramicrotomed sections. Reported higher Fe abundances in IDP GEMS amorphous silicate in some prior works likely reflect either the effects of thermal alteration during atmospheric entry and/or the presence of tiny Fe-bearing inclusions (e.g., Alexander et al., 2017). The analyses in the present study almost certainly also include the occasional undetected metal or sulfide nanocrystal.

4.2. Paris interchondrule matrix and fine-grained rims

Our compositional analyses of amorphous silicate in GEMS-like material in the Paris CM chondrite show slight variations between the ICM and inner and outer FGR. Average Fe content increases slightly from the ICM (Fe/Si $= 0.45 \pm 0.10$) to the outer FGR (Fe/Si $= 0.49 \pm 0.07$) to the inner FGR (Fe/Si $= 0.61 \pm 0.13$), but we note that the composition fields overlap significantly. Given the strong heterogeneity in degree of alteration displayed by Paris, this variation may reflect subtle differences in alteration in addition to any intrinsic differences between ICM and inner and outer FGRs. As such, we want to avoid over-interpretation of the compositional differences we observe. We attribute the somewhat higher Si content in our analyses of amorphous silicates in Paris GEMS-like material compared to those of Leroux et al. (2015) to such local variations, since different petrographic thin sections were analyzed in the respective studies. In the same manner, the slightly higher Mg content in our analyses of amorphous silicates in GEMS-like material in Acfer 094 compared to those of Hopp and Vollmer (2018) may well be due to analysis of different petrographic sections of the chondrite and some variations in composition across it. Hopp and Vollmer (2018) demonstrated compositional variation among FIB sections extracted from a single petrographic section of Acfer 094.

The Paris inner FGR-B has more amorphous silicate and fewer crystalline silicates compared to the outer FGR-A and ICM, in agreement with the findings of Zanetta et al. (2021). While well-ordered phyllosilicates are observed in more altered regions of the Paris ICM, we rarely observed them in the Paris TEM samples in this study, indicating that the 3-chondrule region experienced very limited aqueous alteration. We refer the reader to Villalon et al. (this issue) for additional discussion of Paris FGR and ICM differences.

4.3. Is GEMS-like material in chondrite matrices GEMS?

In identifying material within meteorite matrices as "GEMS-like", past authors have relied on the following properties: near-chondritic (near-solar) elemental composition, amorphous structure of the silicate, morphology (shape), and the presence of Fe-bearing inclusions (e.g., Greshake, 1997; Leroux et al., 2015; Matsumoto et al., 2019; Nittler et al., 2019). Here, we examine how truly like GEMS the amorphous silicates in Paris and Acfer 094 are with respect to each of these properties:

Elemental composition: Although the composition of GEMS grains, including all inclusions, varies greatly from one GEMS grain to another, the average GEMS composition is within a factor of ~2 × solar. Similar near-solar compositions of amorphous silicate-bearing, GEMS-like material in chondrite matrices have been cited as evidence of a possible relationship to GEMS (e.g., Leroux et al. 2015). Our results in Table 1 and Fig. 9 show that, compositionally, the amorphous silicates within GEMS are entirely distinct from those in GEMS-like material in both Paris and Acfer 094 matrices. The amorphous silicates in chondrite GEMS-like material have significantly higher Fe content and narrower Mg content ranges as compared to those in GEMS (Fig. 9). The wider range of Mg contents and very low Fe contents in the amorphous silicate in IDP GEMS likely reflect their unequilibrated state and lack of postaccretional alteration since equilibration would result in heterogeneous compositions, and postaccretional alteration generally results in Fe incorporation in secondary silicates. It is consistent with the nanoscale chemical heterogeneity observed in the past (e.g., Bradley, 1994). When crystalline inclusions are included with the amorphous silicates to obtain bulk GEMS compositions, the composition field in the Mg-Si-Fe ternaries move closer to solar values and overlap with those of the amorphous silicates (without inclusions) in the chondrite matrices. We find that the S content is low, but nonzero, in all of the amorphous silicates (Table 1 and Fig. 9d–f). Sulfur that is present may be due to undetected sulfide inclusions in the analysis regions. Sulfide nano-inclusion sizes in IDP GEMS approach the pixel sizes used to acquire EDS maps, so sulfide inclusions are the likely source of S in IDP GEMS. Sulfur may also be due to small amounts of S-bearing tochilinite; however, we have seen no structural evidence for tochilinite in any of these samples. We also note that Villalon et al. (this issue) report some tochilinite and cronstedtite in TEM sections extracted from a metal-rich region in another Paris petrographic section.

Amorphous structure: The silicate matrix in GEMS in anhydrous IDPs is completely amorphous. There is no evidence for local ordering in their images or FFTs of HRTEM images (Figs. 7 and 8). In contrast, local ordering in the form of fibrous texture was observed in all GEMS-like amorphous silicate in the minimally-altered regions sampled in Paris ICM and FGRs and in Acfer 094 ICM. The fibrous material in amorphous silicate is very electron-beam sensitive; as a result, it disappears with prolonged or high dose electron beam exposure. This suggests that high-current electron beams, not used in this work but often employed for preliminary characterization of meteorite petrographic sections and/or TEM mapping, may destroy poorly crystalline phyllosilicates, leaving only amorphous silicate behind. Thus, care must be taken to obtain accurate results on amorphous silicate-bearing matrices. Even in regions showing only diffuse rings in electron diffraction patterns and in FFTs of HRTEM images, we observed randomly oriented fibers composed of phyllosilicate (Figs. 7 and 8). In the minimally altered region of Paris, short fibers comprised of few-layer packets of phyllosilicates (nanophyllosilicates) were observed, while in more altered regions in Paris, larger and better-ordered phyllosilicates were found. Ferroan serpentine was identifiable in high-resolution imaging of both Paris and Acfer 094 with basal spacing of ~7 Å. The presence of fibers in amorphous silicate, when only diffuse rings in the diffraction pattern or FFT are observed, has been reported previously in Acfer 094 and attributed to minor aqueous alteration (Greshake, 1997; Hopp and Vollmer, 2018). Recent work on clasts with an ultraporous lithology in Acfer 094 matrix clearly shows fibers growing between, as well as sometimes within, nominally amorphous silicate regions (Matsumoto et al., 2019).

In least-altered regions of Paris, fine-scale fibrous texture was previously reported at the edge of GEMS-like amorphous units and in (lower density) pore spaces, and, in moderately altered regions, fibers were identified as cronstedtite-tochilinite intergrowths (Leroux et al., 2015). We observe that the thickness of the conventional FIB-prepared TEM section in that study prevented a clear image of the texture within the amorphous domains in the least-altered Paris matrix region; they may also be comprised of a mixture of amorphous and fibrous textures.

The presence of nanophyllosilicates clearly indicates hydration in both of the chondrite matrices, and the presence of larger phyllosilicate packets in more altered regions of Paris matrix strongly suggests that the fine phyllosilicate fibers in amorphous silicate in minimally altered regions are the result of partial replacement of initially amorphous material. The incomplete replacement is likely due to locally limited water without significant metamorphic reheating in the Paris parent body, as put forth by Hewins et al. (2014). CM chondrites underwent variable low-temperature aqueous alteration resulting in, for example, ~7 wt% H_2O in Murchison (CM2.5), and Paris likewise contains ~5–6 wt% H_2O (Vacher et al., 2020). We observe less nanophyllosilicate in the TEM sections we extracted from Acfer 094 than in those from Paris. This would seem to imply that Acfer 094 is less aqueously altered than Paris, but only a few, limited locations were sampled in each chondrite and, as discussed below, phyllosilicates are sensitive to other kinds of alteration. In Acfer 094, the matrix contains ferrihydrite, proposed to be a product of secondary aqueous alteration (Greshake, 1997) although it may also be due to terrestrial weathering, in addition to amorphous silicates. This study as well as Villalon et al. (this issue) and Matsumoto et al. (2019) observe Fe-(hydro)oxides on the surfaces of mineral grains in Paris and Acfer 094 samples. Rims were also observed in Acfer 094 by Greshake (1997). Matsumoto et al. (2019) attribute these rims to the presence of Fe-rich water. The amorphous silicates in GEMS in IDPs, in contrast, show no evidence for nanophyllosilicates or other evidence for hydration. We discuss below whether GEMS might be the initial amorphous material that was subsequently altered.

Morphology: GEMS in IDPs are partially rounded and are typically ~50–500 nm in diameter. Some form aggregates, but they are generally present as distinct, separated objects as opposed to a continuous structure. In the least-altered Paris ICM studied by Leroux et al. (2015), irregu-

larly shaped domains of amorphous silicate ~100–1000 nm in size were observed. Leroux et al. (1995) cited sub-μm domains of amorphous silicate in support of identification of GEMS-like material. In our observations, we find that the GEMS-like material in Paris has some pore spaces, but the amorphous silicate domains are larger, do not have distinct rounded shapes, and are more connected with each other compared to GEMS in IDPs (Fig. 5b,c and Fig. 6b,d). Villalon et al. (this issue, Supplementary Materials) similarly show amorphous silicate domains in FIB sections of ICM extracted near metal-rich chondrules in Paris that are more connected. The GEMS-like material in Acfer 094 ICM has less pore space and is more continuous than that in Paris (Fig. 5 and Leroux et al., 2015). Neither Paris nor Acfer 094 GEMS-like materials, whether from ICM or FGR regions, have the discrete, partially rounded form of GEMS. These differences between the connectivity of the amorphous silicates in the chondrite matrices and discrete nature GEMS in IDPs are evident in how the samples respond to ultramicrotomy (Fig. 6). The IDP samples microtome cleanly without evidence for fracture of glassy GEMS in the section (although few-μm-sized silicates exhibit some break-up). The esult in the appearance of a preferred fracture direction and the breakup of the GEMS-like material, which indicate that the amorphous silicate regions were large and mechanically connected.

Presence of iron-bearing inclusions: In addition to the amorphous silicate domain size and shape, the presence of opaque inclusions has been cited in support of GEMS-like material identification in chondrites (Leroux et al., 2015; Matsumoto et al., 2019; Nittler et al., 2019). These inclusions result in a "plum pudding" appearance in TEM bright- and dark-field imaging that is similar to that seen in IDP GEMS. Leroux et al. (2015) identified such opaques, tens of nm in diameter, in some GEMS-like objects in least-altered samples of Paris. The reader is referred to the detailed study of the inclusions and their association with the amorphous silicate in Paris matrix provided by Villalon et al. (this issue). We point out that the GEMS in IDPs contain kamacite and pyrrhotite, whereas we did not observe kamacite as inclusions within the amorphous silicate in Paris GEMS-like material and rarely found kamacite inclusions in amorphous silicate in Acfer 094 GEMS-like material. Kamacite, when present in Paris and Acfer 094, was usually found adjacent to sulfide and partially altered. Both pyrrhotite and pentlandite were observed associated with the amorphous silicate in GEMS-like material in Paris and in Acfer 094, consistent with prior work (Greshake, 1997; Leroux et al., 2015; Matsumoto et al., 2019). Pentlandite is commonly thought to be produced during aqueous alteration (e.g., Hewins et al. 2014). Also, the sizes of the opaques do not extend down to the few-nm size scale observed in IDP GEMS.

Iron oxidation state: In addition to the commonly cited points of similarity between GEMS and GEMS-like material in chondrite matrices, we also consider the oxidation state of Fe. In GEMS, the amorphous silicate matrix is nearly Fe-free, and the Fe is present in more reduced forms such as Fe^0 in metal and as Fe^{2+} in sulfide (Fig. 10). Interestingly, we note that whole (bulk) GEMS grains present Fe L-edge EEL spectra that appear dominated by Fe^0 (Fig. 10c) even though sulfides are also present as inclusions and EELS on sulfide inclusions show Fe^{2+} spectra. In the amorphous silicate in GEMS-like material in Paris and Acfer 094 matrices, Fe is present predominantly as Fe^{3+}. Hopp and Vollmer (2018) carried out careful quantitative analyses of Fe oxidation states in Acfer ICM and found $Fe^{3+}/\Sigma Fe = 0.66–0.73$. The similar EEL spectra we observe from Acfer 094 and Paris suggest that Paris ICM has a similarly high Fe^{3+} content. This high oxidation state of Fe is consistent with the observation of oxide rims on metal and sulfide grains (Villalon et al., this issue). The process resulting in the high oxidation state of Fe is most likely the aqueous alteration that also generated fine fibers of phyllosilicate in the minimally altered regions of Paris and larger and better-crystallized phyllosilicates in more altered regions.

We also consider the association of the amorphous silicate with organic carbon. In GEMS-rich IDPs, GEMS are typically fully embedded in organic carbon, contain variable amounts of carbon throughout their interiors, and some GEMS are composites of organic carbon and amorphous silicate (Ishii et al., 2018). The carbon also acts as a glue connecting GEMS with other components. Fig. 11 shows some examples of organic carbon associated with amorphous silicate GEMS. GEMS-rich IDPs typically contain as much as 10–20 × more organic carbon by volume than bulk chondrites. Carbon abundances in anhydrous chondritic IDPs are, on average, ~13 wt%, while GEMS-rich IDPs tend to have more carbon, approaching ~45 wt % (Bradley, 2014). Rough estimates of the abundance of carbon in the matrices of Paris and Acfer 094 based on bulk carbon abundances in CM chondrites and in Acfer 094 (Krot et al., 2014), estimates of the volume fraction of matrix in each case (Hewins et al., 2014; Krot et al., 2014), and an oversimplified assumption that carbon resides entirely in the matrix indicate that there is as much as ~10 wt% carbon in Paris matrix and ~2 wt% in Acfer 094 matrix. In a FIB section of amorphous silicates in minimally altered Paris ICM, Leroux et al. (2015) showed some sub-μm regions of patchy carbon between amorphous silicate domains and thin, discontinuous carbonaceous material on some domains. (A comparison of their C map to those in Fig. 11 is illustrative of the differences in carbon abundance.) We note that the abundance of carbon in this study is high, because GEMS-rich IDPs were selected—GEMS-poor IDPs tend to have somewhat lower carbon content, but even those are typically more carbon-rich than the chondrite ICM.

A final important difference is that, compared to Paris or Acfer 094 matrix, GEMS-rich IDPs have higher abundances of presolar silicates, albeit with higher uncertainties due to the lower volume of samples analyzed. See Villalon et al. (this issue) for a discussion of the implications of this for Paris. We note that the population of anhydrous IDPs almost certainly comes from multiple parent bodies, complicating direct comparisons of presolar grain abundances with meteorite samples form single parent bodies.

Nonetheless, the presolar silicate abundance in Acfer 094 matrix is ~200 ppm, a factor of ~2 × lower than that in anhydrous IDPs and as much as ~10–75 × lower than in the ultraprimitive IDPs collected from the comet 26P/Grigg-Skjellerup dust stream (Busemann et al., 2009; Vollmer et al., 2009a; Davidson et al., 2012; Floss and Haenecour, 2016). Recent analyses of Paris indicate far lower presolar silicate abundances of ~12 ppm in the least-altered lithology (Verdier-Paoletti et al., 2019). Based on all of the comparisons above, we find that the GEMS-like material in the matrices of Paris and Acfer 094 are not equivalent to the GEMS in anhydrous chondritic IDPs. Indeed, the description of "GEMS-like" is superficial since GEMS in IDPs are significantly less altered than the GEMS-like material in chondrite matrix.

4.4. Possible origins of GEMS-like material in chondrite matrices

Having concluded that GEMS-like material in the Paris and Acfer 094 matrices is not GEMS as found in anhydrous IDPs, we now ask if the GEMS-like material was GEMS that subsequently altered or if it has an origin independent of GEMS. Several possible origins for the amorphous silicates in chondrite matrices have been considered. These include pre-accretionary alteration of individual GEMS, accretion of *bona fide* GEMS, accretion of rapidly condensed amorphous silicate generated by high temperature events prior to accretion, shock melting on the parent body, and formation as a product of parent-body alteration of already-accreted components on the parent body. Although Paris is a breccia, we can immediately rule out shock-induced melting in both Paris and Acfer 094 since the amorphous silicate does not appear as melt veins, pockets, dikes, or in mineral fractures in either chondrite. Additional arguments against shock-induced melting that are appropriate to these chondrites are enumerated in Brearley (1993).

Next, we consider whether the GEMS-like material we observe in the matrices and FGRs of Paris and Acfer 094 might have been GEMS originally. The presence of a low-Fe, Mn-enriched (LIME) forsterite ribbon, consistent with direct condensation from a solar composition gas, and carbonaceous nanoglobules have been noted in Paris (Villalon et al., this issue). These phases have also been identified in GEMS-rich IDPs, suggesting a possible common source for the amorphous silicates. If the amorphous silicates in GEMS-like material in the Paris and Acfer 094 matrices were originally GEMS, then prior to or since accretion in their respective parent bodies, the GEMS amorphous silicate must have undergone the following:

- The GEMS amorphous silicate must have altered in such a manner that its composition became more homogeneous and, on average, much more Fe-rich.
- The GEMS must have compacted to generate larger amorphous silicate domains with less distinct boundaries, yet still maintain open pore spaces.
- The original population of small Fe-bearing opaques must have been removed, presumably by alteration.
- Significant amounts of organic carbonaceous material must have been lost.
- The material must have experienced hydration and an increase in the oxidation state of Fe.
- The abundance of presolar silicates must have decreased.

We consider first whether GEMS-like material might be formed by alteration of free-floating GEMS grains in the nebula prior to accretion on a parent body. Pre-accretionary aqueous alteration has been proposed in CO3.0 chondrites based on identical presolar SiC abundances but different presolar silicate abundances in FGRs and ICM (Haenecour et al. 2018). We consider an unspecified process that resulted in homogenized composition but did not involve destruction of GEMS and recondensation of amorphous material. (Recondensation of amorphous material is considered below.) Individual GEMS grains in IDPs display a wide range of bulk compositions, including huge variation in Fe content. The Fe content of bulk GEMS grains extends to levels below the lowest Fe content, but not up to the highest Fe content, observed in the amorphous silicates in GEMS-like material in Paris and in Acfer 094 chondrite matrices (Fig. 9). Homogenizing individual GEMS grains (or even aggregates of a few) would be expected to produce similar compositional heterogeneity within GEMS-like material, including regions of Fe content lower than observed. Iron content in the amorphous silicate in GEMS-like material that is higher than bulk GEMS compositions is also problematic in this scenario, especially since the GEMS-like material contains additional Fe in mineral inclusions. Thus, pre-accretionary processing of GEMS grains cannot explain the observed homogeneity in compositions of amorphous silicate within GEMS-like materials, and although it may have occurred, a mechanism of incorporating additional Fe into the amorphous silicate matrix of the GEMS-like material would also be required.

We also consider whether GEMS may have accreted and been subsequently altered on the parent body to form GEMS-like material, a possibility supported by the presence, even in the least-altered regions from which we extracted TEM samples, of pentlandite, calcium carbonate and possible sulfate (Figs. 3 and 4), and nanophyllosilicate (Fig. 8). It may be possible to hydrate amorphous silicates on the parent body to form an amorphous gel under conditions that inhibit crystallization (Howard et al., 2011). It is also possible that aqueous alteration, in addition to hydration, could destroy the finest grain size of Fe-bearing opaques and introduce additional Fe into the surrounding amorphous silicate from other sources. Aqueous processing is expected to dilute the presolar signature of a large fraction of presolar silicates, including presolar GEMS, leading to reduced abundance of presolar silicates. Aqueous alteration could also redistribute and dilute organics, but consideration of bulk C contents suggests a large amount of carbon must also have been lost. It is very unlikely, however, that aqueous processing and mild thermal metamorphism can generate such uniform compositions as we observe under conditions in which water was sufficiently limited that heterogeneity in the degree of alteration

resulted. To distribute Fe uniformly over the ~10 μm we observe in our TEM samples requires its transport and incorporation into the amorphous silicate over those length scales without significant crystallization of the amorphous silicate. We and other authors have noted the presence of sub-μm to multi-μm-sized sulfides, including pentlandite (Hewins et al. 2014; Leroux et al. 2015). Pentlandite develops with progressive aqueous alteration (e.g., Abreu and Brearley, 2010; Singerling and Brearley, 2020), and the growth of secondary phases similarly requires considerable transport to occur. Such transport around and through amorphous GEMS while retaining their amorphous structure is unlikely.

Regarding alteration to GEMS shapes and sizes, compaction on the parent body can be invoked to combine GEMS, with their smaller sizes, into larger domains with more irregular shapes and less distinct boundaries; however, it remains difficult to construct a scenario in which compaction also maintains the abundant open pore spaces observed in Paris GEMS-like material (Leroux et al., 2015). We find it more likely that GEMS-like domains were not initially smaller. Aggregation of GEMS prior to accretion also still fails to address the challenges of differing composition and the structural changes expected to accompany a process, like hydrothermal alteration, that can increase the Fe content in the amorphous silicate. To summarize, GEMS as the (direct) precursor materials for GEMS-like material in these chondrite matrices cannot be ruled out, but we find it unlikely based on the considerations above.

Another possible origin for the amorphous silicates in GEMS-like material in Paris and Acfer 094 chondrite matrices is that they formed from the accretion of rapidly condensed materials formed in a transient high-temperature event like the chondrule-forming event. Such an event might have also destroyed (or partially destroyed) GEMS grains, if they were present, and would permit addition of greater quantities of Fe in resultant amorphous silicate material via co-vaporization of other Fe-rich objects. Abreu and Brearley (2010) studied matrices of CR chondrites that escaped preterrestrial aqueous alteration and observed amorphous silicate compositions even more Fe-rich than those we see in Acfer 094 and Paris. They remarked on the similarities to Acfer 094 matrix. Because they did not find evidence for aqueous alteration and oxidation, they concluded that the amorphous silicate and nanosulfide particles that dominate the matrices formed by rapid condensation in a high temperature event prior to accretion. Greshake (1997) also considered this as a possible origin for Acfer 094 amorphous silicates. In this scenario, the amorphous silicates are accreted with relatively high Fe contents generated by vaporization of Fe-bearing phases in addition to silicate and rapid recondensation and, thus, do not require a parent body alteration process to redistribute Fe from inclusions into the amorphous silicate matrix. They must, however, remain amorphous (or at least, largely disordered) since accretion. Rapid condensation of vaporized nebular solids would also be consistent with the dearth of presolar silicates in Paris (Verdier-Paoletti et al., 2020) but is less consistent with the higher presolar silicate abundances seen in Acfer 094, although accretion of varying proportions of recondensed amorphous silicate and nonvaporized nebular dust might be invoked to explain these differences. The scenario of amorphous silicate formation by rapid condensation in a transient high-temperature event is a possibility for the origin of GEMS-like material in the Paris and Acfer 094 matrices but remains unsatisfyingly unconstrained in terms of environment and formation conditions.

Finally, we consider that the amorphous silicates in GEMS-like material in Paris and Acfer 094 matrices may have formed as a product of parent-body alteration of already-accreted components on the parent body that were not necessarily GEMS. Like rapid condensation, parent-body alteration, particularly aqueous processing, would be consistent with the low abundances of presolar silicates detected in Paris. Unlike in the case made for the CR chondrites studied by Abreu and Brearley (2010), there is evidence of aqueous alteration in both Acfer 094 and Paris matrices (Bischoff and Geiger, 1995; Rubin, 2015). In Paris, in particular, we see evidence for aqueous alteration, even of the round pristine-metal-bearing Type I chondrule bordering the region of Paris from which TEM sections were extracted. Oxidation of outer rims of metal, replacement of mesostasis with phyllosilicates, and vein filling with secondary carbonates and sulfates are some examples (Fig. 3). Secondary pentlandite, carbonate and possible sulfate are also present in the ICM (Fig. 3), indicating the presence of water where GEMS-like material resides. The high oxidation state of Fe in the amorphous silicate in GEMS-like material from both Paris and Acfer 094 matrix is also consistent with aqueous processing. The water-limited conditions for alteration in Paris that resulted in heterogeneous degree of aqueous processing would have resulted from local microchemical environments as observed in other CM chondrites (Brearley, 2014). It is unclear what those environments were and whether they could produce amorphous silicates as hydrated gels, perhaps via water vapor instead of liquid. The role of aqueous processing in amorphous silicate formation, alteration, and destruction still remains poorly understood.

There is also petrographic evidence for brecciation and impact crushing in Paris (Rubin, 2015). As expected for a lithified object, Acfer 094 has similarly experienced impact processing (Wasson and Rubin, 2010). The finding of amorphous silicate with diopside composition in Paris outer FGRs (Figs. 6i and j, Electronic Annex Fig. S12) strongly suggests a shock origin for at least some of the amorphous silicate in that chondrite. Local shock states can vary greatly in heterogeneous media like chondrite matrix (Rutherford et al., 2017), possibly allowing for survival of some silicates and amorphization of others.

Impact processing and aqueous processing are likely to operate in tandem. Collisional processing has been proposed to facilitate aqueous alteration on the CM parent body by impact-mobilization of water and preferential alteration of the more strongly shocked regions (Rubin, 2012). The evidence for impact processing in Paris raises the intriguing possibility that shock processing may have acted to amorphize phyllosilicates (e.g., Harries et al., 2020) that were generated by prior aqueous alteration,

either on the Paris CM parent body or prior to accretion. Both Paris and Acfer 094 are classified as having S1 shock stage (Stöffler et al., 1991); however, shocks of less than about 5 GPa are not detectable in olivine extinction features in thin sections. Structural degradation of phyllosilicates begins at pressures of only a few GPa in dynamic compression experiments (Harries et al., 2020), and multiple impact events may be expected to have additive effects. Gradual recrystallization in low-water environments following shock may generate the nanophyllosilicate fibrous textures observed in the least-altered regions of Paris matrix. Thus, parent-body alteration processes on the parent body may also play a role in the formation of amorphous silicates and GEMS-like material in chondrite matrices, and we plan to evaluate this possibility in more detail in future work.

4.5. the question of presolar GEMS-like material in chondrites

Presolar GEMS grains, dominated by amorphous silicates, have been unambiguously identified in anhydrous IDPs (e.g., Messenger et al., 2003; Floss et al., 2006). In these cases, the GEMS grains were first identified by TEM methods and then analyzed by SIMS methods, usually NanoSIMS. This order of analysis ensures that the amorphous regions lacking crystalline structure are characterized and their locations are known in advance of any subsequent processing or analyses that might damage crystal structure, like SIMS analysis. In contrast, published reports of amorphous silicates identified as presolar in chondrite matrices first apply SIMS analyses in order to identify isotopically anomalous regions. In many cases, isotopically anomalous grains have been subsequently analyzed only for elemental chemistry. Considering prior work on Acfer 094 matrix, for example, Nguyen and Zinner (2004) identified a "candidate for a GEMS" in Acfer 094 based on excess O and high Fe content as determined by SEM-EDS. Vollmer et al. (2009a) identified a "GEMS-like grain" in Acfer 094 by its (Mg + Fe)/Si ratio, incompatible with pyroxene or olivine, and elevated S content using Auger electron spectroscopy. Amorphous structure in individual small grains can only be established using electron diffraction-based methods (via image contrast and/or Bragg scattering), but in neither case was structural data presented that demonstrates the anomalous region was amorphous, critical in assigning "GEMS-like" character.

Other reports of amorphous silicates identified as presolar in Acfer 094 matrix involve preparation of FIB sections and TEM analysis following initial SIMS analyses. These permit structural analysis but suffer from uncertainties introduced by sample preparation and analysis methods that may have amorphized previously crystalline silicates. The NanoSIMS analysis itself amorphizes the remaining top ~10–30 nm of the sample. That is sometimes all that remains of grains of interest, especially after multiple rounds of NanoSIMS analysis (e.g. Nguyen et al., 2016). During Auger nanoprobe electron spectroscopy, often used to obtain grain composition in conjunction with NanoSIMS, long duration analyses in small areas can induce major electron beam damage that can even sputter away of material. Auger-induced holes in an amorphous or weakly crystalline silicate grain were observed by Vollmer et al. (2009b). FIB-isolation, in which a focused ion beam is used to mill away surrounding material for reduced isotopic dilution from nearby matrix grains in subsequent NanoSIMS analyses, may also result in grain amorphization. Because the tails of the FIB ion beam interact with the target grain during the FIB-isolation process, amorphized material depth may extend below that generated by the SIMS analyses themselves. Of six presolar silicate grains identified as amorphous by Nguyen et al. (2016), four had been prepared by FIB-isolation, and of those, two had only ~10–20 nm of the presolar grain remaining at the time of TEM analysis, and one (grain 2_4) had a diffraction pattern indicative of nanocrystals. The FIB milling processing during extraction of an electron-transparent section for TEM also carries the potential for amorphization as well as redeposition of nonstoichiometric amorphous material. IDPs are commonly prepared by ultramicrotomy instead of FIB methods, so amorphous artifacts of FIB preparation are not a factor in studies of GEMS in anhydrous IDPs. Finally, there is the potential for amorphization of some beam-sensitive silicates in the TEM, a risk to both IDPs and to meteorite matrix samples.

For sufficiently large amorphous grains, these uncertainties as to whether amorphous structure is indigenous can be reduced. Nguyen et al. (2007) used FIB extraction (without FIB-isolation) and TEM to study an isotopically anomalous silicate grain ~500 nm in size in Acfer 094. The grain was initially identified as clinopyroxene based on SEM-EDS and was found by TEM to contain Si, O, Mg, Fe, Al, and Ca. The Ca/Si ratio, based on relative abundances in the TEM-EDS spectrum shown in Nguyen et al. (2007), is significantly higher than that reported in Table 1 for the amorphous silicates in GEMS-like material from Acfer 094. Diffraction data were not provided, but the grain was reported to be amorphous. The smooth texture of the bright field TEM image suggests there are no inclusions of metal or sulfides in the grain, so it is not GEMS-like. Six presolar silicates in Acfer 094 matrix were identified as amorphous by FIB and TEM by Nguyen et al. (2016), some using FIB-isolation, as discussed above. One of those was reported to be GEMS-like with FeNi metal inclusions in Fe-rich amorphous silicate. Sulfur was not reported. Unfortunately, only ~10 nm of the grain remained, a thickness processed by the NanoSIMS sputtering process. Vollmer et al. (2009b) also identified presolar silicate grains in Acfer 094 matrix, demonstrated to be amorphous by TEM electron diffraction. One of those contains ~50 nm Fe-rich minerals in amorphous silicate and a bulk composition that is Fe-rich (Fe/Si 0.88–0.97) and contains sulfur. Vollmer et al. (2009b) identify it as classical GEMS with a cautionary note that the TEM section may not have been extracted precisely at the presolar grain location. While the grain may appropriately be called "GEMS-like", we note that it is far more Fe-rich than bulk GEMS in IDPs (Fig. 9c and Keller and Messenger, 2011).

GEMS-like presolar silicates have been reported in other meteorite matrices as well. For example, Nittler et al. (2019)

recently identified O isotope anomalies in a carbon-rich clast in LAP 02,342 (CR2) and used FIB extraction from a ^{16}O-poor region and TEM to study amorphous silicate grains that they identified as GEMS due to the presence of Fe-bearing inclusions. Bradley (2019) disputed their identification as GEMS, and they are more appropriately described as "GEMS-like".

To date, only a few presolar silicate grains from Acfer 094 have been identified, demonstrated to be structurally amorphous, and are sufficiently large that amorphization from pre-TEM processing can be eliminated. Because Paris is a recent find, limited analyses of presolar grains have been performed to date. Future studies carried out with structural identification of the amorphous silicates prior to NanoSIMS, in the same order of analysis typically used for anhydrous IDPs, would represent a valuable contribution to the understanding of amorphous silicates in primitive chondrite matrices. Since Acfer 094 matrix has approximately half the abundance of presolar grains in anhydrous IDPs, twice the sample area would need to be analyzed to obtain similar statistics.

To date, not a single presolar grain with the requisite properties of GEMS, i.e., kamacite and pyrrhotite nanoinclusions in Fe-poor (<5 at%), amorphous silicate groundmass, has been unambiguously identified in any meteorite. It remains unclear why this is the case. Perhaps sufficiently preserved meteorite matrix has yet to be identified, and studies of even less altered chondrite matrices may shed new light on the origin of GEMS-like material. Alternatively, evidence of GEMS may have been efficiently erased during parent body alteration. Finally, GEMS may not have survived the energetic inner nebula environment intact, unlike more robust and refractory presolar grains including some crystalline silicates.

4.6. Rethinking the implicit assumption that amorphous silicates indicate primitivity and pristinity

Reports that suggest that presolar amorphous silicates accreted as amorphous grains and have been preserved since in their amorphous state, are necessarily speculative since grain structure may conceivably be altered without massive dilution of isotope anomalies (Nguyen and Zinner, 2004; Vollmer et al., 2009a,b; Nittler et al., 2019; Bradley, 2019). Even so, there has been a tendency in the literature to associate the presence of "GEMS-like" amorphous silicate material in meteorite matrices with both primitivity and pristinity of the sample, an implicit assumption of survival of original accreted amorphous solids. It is certainly the case that many of the meteorites with amorphous silicates in their matrices do boast high presolar grain abundances and other characteristics indicative of mild parent body alteration. Acfer 094 is a prime example: due to its high abundances of presolar silicates, SiC and diamond (Newton et al. 1995; Vollmer et al. 2009a) and the presence of amorphous silicates (among other characteristics), it has commonly been described as highly primitive and presumed to be pristine. While its high abundances of presolar grains warrant the moniker of "primitive", it is not pristine, having experienced impact processing and aqueous alteration as well as terrestrial weathering. The survival of presolar SiC and diamond is, however, an indication of minimal thermal metamorphism, which progressively destroys these grains (Huss and Lewis, 1995).

The generally favored explanation for amorphous silicate presence in chondrite matrices is rapid condensation of vapor in a transient heating event in the solar nebula, like the chondrule-forming event(s), prior to accretion. This explanation has the advantage of enabling the high and uniform Fe contents of the amorphous silicates in chondrite matrices, as discussed above. In cases like Acfer 094 where abundant presolar silicates are associated with amorphous silicates in the matrix, a high temperature formation scenario for the amorphous silicates is less convincing. Whatever formation mechanism is invoked, given the highly nonequilibrium nature of amorphous materials, the likelihood of amorphous silicate survival over ~4.5 Ga in their original (or nearly original) amorphous state as they undergo the processes of accretion, compaction, and subsequent impact, aqueous, and (mild) thermal processing is low. Amorphous silicates are inherently fragile and sensitive to even weak or mild alteration. Refractory presolar grains, like the presolar SiC and diamond found in high abundances in Acfer 094, resist aqueous alteration and even chemical attack by acids used in extracting them from bulk matrix. Even presolar crystalline silicates, while less resistant to alteration, are far less sensitive than amorphous silicates.

It is thus important to recognize that the presence of amorphous silicates in a matrix, on its own, does not support a verdict of pristinity for the host meteorite. Primary amorphous silicate grains, i.e., amorphous at the time of accretion onto their parent body, with nonsolar isotopic compositions have yet to be rigorously identified in the matrix of any carbonaceous chondrite. There are many mechanisms to produce amorphous structure in silicates. These include processes requiring high temperature excursions, like melt-quenching and rapid condensation from a vapor. Other processes, like shock processing and hydrous gel formation during aqueous processing (Harries et al., 2020; Howard et al., 2011), can operate efficiently without huge temperature excursions. Hydrous gel formation can produce amorphous silicates by direct alteration of anhydrous precursors or by alteration of already-hydrated phases. Fluid mobilization acts to homogenize compositions of the resulting hydrated amorphous silicate. Many of the recognized products of secondary aqueous alteration, like phyllosilicates and ferrihydrite, are also fragile in the face of other kinds of processing. Changes in chemical environment in aqueous processing can destabilize phyllosilicate structures resulting in amorphous silicates (e.g., Howard et al., 2011). Shear stresses from impacts with relatively low pressures of a few GPa can initiate amorphization of phyllosilicates and partially devolatilize hydrous phases. We do not claim that all amorphous silicates, including GEMS-like material, in chondrite matrices necessarily formed as a result of secondary alteration processes; however, even if originally-amorphous material accreted on a chondrite parent body (whether *bona fide* GEMS or rapidly condensed vapor from reprocessed precursor material), because episodes of aqueous alteration and mild

thermal metamorphism can be interspersed with (low-pressure) collisional shock processing over the lifetime of the parent body, it may be impossible to fully constrain amorphous silicate origins in chondrite matrices. The likely presence of at least some presolar and currently-amorphous silicate in the matrix of Acfer 094 indicates that, if the amorphous structure of that silicate is the result of parent body processing, then this meteorite experienced sufficiently mild alteration that some isotope anomalies in silicates were not diluted beyond detection.

5. CONCLUSIONS

To further our understanding of GEMS-like material (amorphous silicate with inclusions) in the matrices of chondrites, we have applied a new combined FIB-ultramicrotomy method, developed specifically for the study of fine-grained meteoritic materials, to produce and study ultrathin TEM sections containing amorphous silicate from Acfer 094 and the minimally altered, metal-rich lithology in Paris. In Paris, we sampled the ICM and inner and outer FGRs. We compared the GEMS-like material in these chondrites to the GEMS in anhydrous cometary-type IDPs, focusing particularly on the morphology, degree of partial ordering, elemental composition, and dominant Fe oxidation state in the amorphous silicate itself. From these data, we assessed the likelihood that the GEMS-like material in the chondrite matrices is GEMS, was GEMS that was subsequently altered, or has an origin independent of GEMS. We find that the GEMS-like material in Paris and Acfer 094 chondrite matrices is not GEMS. The amorphous silicate in GEMS is fully amorphous, Fe-poor, and shows no signs of hydration. The GEMS-like materials in Paris and Acfer 094 show incipient ordering and are Fe-rich, highly oxidized, and hydrated. Although it is possible that GEMS-like material in Paris and Acfer 094 formed by accretion and subsequent alteration of GEMS, it is unlikely that the necessary alterations to GEMS could be achieved without more advanced crystallization of the amorphous silicate and loss of porosity as well as a loss of smaller-sized presolar silicate grains. It is particularly challenging to explain the required loss of carbon from the system and the uniform chemical compositions of amorphous silicate observed in the chondrite matrices by alteration of primary GEMS. Rapid condensation in a transient, high temperature event like the chondrule-forming event is a possible formation route but requires preservation of large quantities of amorphous silicate since accretion. Complex alteration processes involving weak aqueous alteration and shock processing of already-accreted chondrite components are also possible explanations for the origins of the amorphous silicates in Acfer 094 and Paris that warrant further exploration by TEM methods. We conclude that the presence of GEMS-like amorphous silicates in a chondrite matrix is not a reliable indicator for high degrees of primitivity or pristinity. We advocate for future searches for presolar amorphous silicates using samples of chondrite matrix precharacterized by TEM methods to enable direct comparisons to anhydrous IDP presolar GEMS abundances.

Declaration of Competing Interest

The authors declare that they have no known competing financial interests or personal relationships that could have appeared to influence the work reported in this paper.

ACKNOWLEDGEMENTS

The authors thank D. Brownlee and D. Joswiak for providing ultramicrotomed sections of several anhydrous IDPs and the polished section of the Acfer 094 meteorite studied in this work. The Museum National d'Histoire Naturelle in Paris, France is also gratefully acknowledged for the loan of the Paris meteorite polished section. This manuscript benefited greatly from detailed reviews and constructive comments by Ashley King and two anonymous reviewers. Work at the Molecular Foundry was supported by the Office of Science, Basic Energy Sciences, U.S. Department of Energy under Contract No. DE-AC02-05CH11231. This research was funded by NASA grants NNX16AK41G and 80NSSC19K0936 to Ishii, 80NSSC17K0251 to Davis, and 80NSSC17K0494 to Villalon. Ciston acknowledges additional support from the Presidential Early Career Award for Scientists and Engineers (PECASE) through the U.S. Department of Energy.

APPENDIX A. SUPPLEMENTARY MATERIAL

Supplementary data to this article can be found online at https://doi.org/10.1016/j.gca.2021.05.042.

REFERENCES

Abreu N. M. and Brearley A. J. (2010) Early solar system processes recorded in the matrices of two highly pristine CR3 carbonaceous chondrites, MET 00426 and QUE 99177. *Geochim. Cosmochim. Acta.* **74**, 1146–1171.

Alexander C. M. O'D., Hutchison R. and Barber D. J. (1989) Origin of chondrule rims and interchondrule matrices in unequilibrated ordinary chondrites. *Earth Planet. Sci. Lett.* **95**, 187–207.

Alexander C. M. O. D., Nittler L. R., Davidson J. and Ciesla F. J. (2017) Measuring the level of interstellar inheritance in the solar protoplanetary disk. *Meteorit. Planet. Sci.* **52**, 1797–1821.

Bischoff A. and Geiger T. (1995) Meteorites from the Sahara: Find locations, shock classification, degree of weathering and pairing. *Meteoritics* **30**, 113–122.

Bradley J. P. and Brownlee D. E. (1986) Cometary particles: Thin sectioning and electron beam analysis. *Science* **231**, 1542–1544.

Bradley J. P. (1994) Chemically anomalous, preaccretionally irradiated grains in interplanetary dust from comets. *Science.* **265**, 925–929.

Bradley J. P. (2014) Early solar nebula grains – interplanetary dust particles. In Meteorites and Cosmochemical Processes (ed. A. M. Davis), Vol. 1 Treatise on Geochemistry, 2nd Ed. (Exec. Eds. H. D. Holland and K. K. Turekian). Elsevier, Oxford, pp. 287–308.

Bradley J. P. (2019) GEMS and the devil in their details. *Nature Astron.* **3**, 603–605.

Brearley A. J. (1993) Matrix and fine-grained rims in the unequilibrated CO_3 chondrite, ALHA 77307: origins and evidence for diverse, primitive nebular dust components. *Geochim. Cosmochim. Acta* **57**, 1521–1550.

Brearley A. J. (2014) Nebular versus parent body processing. In Meteorites and Cosmochemical Processes (Ed. A. M. Davis),

Vol. 1 Treatise on Geochemistry, 2nd Ed. (Exec. Eds. H. D. Holland and K. K. Turekian). Elsevier, Oxford, pp. 287–308.

Brownlee D. E., Joswiak D. J. and Bradley J. P. (1999) High spatial resolution analyses of GEMS and other ultrafine grained IDP components. *Lunar Planet. Sci.* **30**, #2031.

Busemann H., Nguyen A. N., Cody G. D., Hoppe P., Kilcoyne A. L. D., Stroud R. M., Zega T. J. and Nittler L. R. (2009) Ultra-primitive interplanetary dust particles from the comet 26P/Grigg-Skjellerup dust stream collection. *Earth Plan. Sci. Lett.* **288**, 44–57.

Chizmadia L. J. and Brearley A. J. (2008) Mineralogy, aqueous alteration, and primary textural characteristics of fine-grained rims in the Y-791198 CM2 carbonaceous chondrite: TEM observations and comparison to ALHA81002. *Geochim. Cosmochim. Acta* **72**, 602–625.

Cuvillier P., Chaumard N., Leroux H., Zanda B., Hewins R. H., Jacob D. and Devouard B. (2018) A TEM study of exsolution in Ca-rich pyroxenes from the Paris and Renazzo chondrites: Determination of type I chondrule cooling rates. *Meteorit. Planet. Sci.* **53**, 482–492.

Davidson J., Busemann H. and Franchi I. A. (2012) A NanoSIMS and Raman spectroscopic comparison of interplanetary dust particles from comet Grigg-Skjellerup and non-Grigg Skjellerup collections. *Meteorit. Planet. Sci.* **47**, 1748–1771.

Dobrică E. and Brearley A. J. (2020) Amorphous silicates in the matrix of Semarkona: The first evidence for the localized preservation of pristine matrix materials in the most unequilibrated ordinary chondrites. *Meteorit. Planet. Sci.* **55**, 649–668.

Dobrică E., Engrand C., Leroux H., Rouzaud J.-N. and Duprat J. (2012) Transmission electron microscopy of the CONCORDIA UltraCarbonaceous Antarctic MicroMeteorites (UCAMMs): Mineralogical properties. *Geochim. Cosmochim. Acta* **76**, 68–82.

Ebel D. S., Brunner C., Konrad K., Leftwich K., Erb I., Lu M., Rodriguez H., Crapster-Pregont E. J., Friedrich J. M. and Weisberg M. K. (2016) Abundance, major element composition and size of components and matrix in CV, CO and Acfer 094 chondrites. *Geochim. Cosmochim. Acta* **172**, 322–356.

Floss C. and Haenecour P. (2016) Presolar silicate grains: Abundances, isotopic and elemental compositions, and the effects of secondary processing. *Geochem. J.* **50**, 3–25.

Floss C., Stadermann F. J., Bradley J. P., Dai Z. R., Bajt S., Graham G. and Lea A. S. (2006) Identification of isotopically primitive interplanetary dust particles: a NanoSIMS isotopic imaging study. *Geochim. Cosmochim. Acta* **70**, 2371–2399.

Greshake A. (1997) The primitive matrix components of the unique carbonaceous chondrite Acfer 094: A TEM study. *Geochim. Cosmochim. Acta.* **61**, 437–452.

Haenecour P., Floss C., Zega T. J., Croat T. K., Wang A., Jollif B. L. and Carpenter P. (2018) Presolar silicate in the matrix and fine-grained rims around chondrules in primitive CO3.0 chondrites: Evidence for pre-accretionary aqueous alteration on the rims in the solar nebula. *Gecochim. Cosmochim. Acta* **221**, 379–405.

Harries D., Schmidt D., Fazio A., Wild P., Liermann H.-P. and Langenhorst F. (2020) Space weathering of phyllosilicates by hypervelocity impact: Experimental insights into serpentine amorphization by non-hydrostatic stresses. *Lunar Planet. Sci.* **51**, #2273.

Hewins R. H., Bourot-Denise M., Zanda B., Leroux H., Barrat J.-A., Humayun M., Goepel C., Greenwood R. C., Franchi I. A., Pont S., Lorand J.-P., Cournède C., Gattacceca J., Rochette P., Kuga M., Marrocchi Y. and Marty B. (2014) The Paris meteorite, the least altered CM chondrite so far. *Geochim. Cosmochim. Acta* **124**, 190–222.

Hopp T. and Vollmer C. (2018) Chemical composition and iron oxidation state of amorphous matrix silicates in the carbonaceous chondrite Acfer 094. *Meteorit. Planet. Sci.* **53**, 153–166.

Hoppe P., Leitner J. and Kodolányi J. (2017) The stardust abundance in the local interstellar cloud at the birth of the Solar System. *Nature Astron.* **1**, 617–620.

Howard K. T., Benedix G. K., Bland P. A. and Cressey G. (2011) Modal mineralogy of CM chondrites by X-ray diffraction (PSD-XRD): Part 2. Degree, nature and settings of aqueous alteration. *Geochim. Cosmochim. Acta* **75**, 2735–2751.

Huss G. R. and Lewis R. S. (1995) Presolar diamond, SiC, and graphite in primitive chondrites: Abundances as a function of meteorite class and petrologic type. *Geochim. Cosmochim. Acta* **59**, 115–160.

Ishii H. A., Krot A. N., Bradley J. P., Keil K., Nagashima K., Teslich N., Jacobsen B. and Yin Q.-Z. (2010) Discovery, mineral paragenesis, and origin of wadalite in a meteorite. *Amer. Mineral.* **95**, 440–448.

Ishii H. A., Bradley J. P., Bechtel H. A., Brownlee D. E., Bustillo K. C., Ciston J., Cuzzi J. N., Floss C. and Joswiak D. J. (2018) Multiple generations of grain aggregation in different environments preceded solar system body formation. *Proc. Natl. Acad. Sci.* **115**, 6608–6613.

Jin Y., Xu H. and Abhaya K. D. (2006) Electron energy loss spectroscopy (EELS) of iron Fischer-Tropsch catalysts. *Microscopy Microanal.* **12**, 124–134.

Jones A. P., Fanciullo L., Kohler M., Verstraete L., Guillet V., Bocchio M. and Ysard N. (2013) The evolution of amorphous hydrocarbons in the ISM: dust modelling from a new vantage point. *Astron. Astrophys.* **558**. A62 (22 pp).

Keller L. P., Messenger S. and Bradley J. P. (2000) Analysis of a deuterium-rich interplanetary dust particle (IDP) and implications for presolar material in IDPs. *J. Geophys. Res. Space Phys.* **105**, 10397–10402.

Keller L. P. and Messenger S. (2011) On the origins of GEMS grains. *Geochim. Cosmochim. Acta* **75**, 5336–5365.

Kemper F., Waters L. B. F. M., de Koter A. and Tielens A. G. G. M. (2001) Crystallinity versus mass-loss rate in asymptotic giant branch stars. *Astron. Astrophys.* **369**, 132–141.

Kemper F., Vriend W. J. and Tielens A. G. G. M. (2004) The absence of crystalline silicates in the diffuse interstellar medium. *Astrophys. J.* **609**, 826–837.

Krot A. N., Keil K., Scott E. R. D., Goodrich C. A. and Weisberg M. K. (2014) In Meteorites and Cosmochemical Processes (ed. A. M. Davis), Vol. 1 Treatise on Geochemistry, 2nd Ed. (Exec. Eds. H. D. Holland and K. K. Turekian). Elsevier, Oxford, pp. 1–63.

Le Guillou C., Changela H. G. and Brearley A. J. (2015) Widespread oxidized and hydrated amorphous silicates in CR chondrite matrices: Implications for alteration conditions and H2 degassing of asteroids. *Earth Planet. Sci. Lett.* **420**, 162–173.

Leroux H., Cuvillier P., Zanda B. and Hewins R. H. (2015) GEMS-like material in the matrix of the Paris meteorite and the early stages of alteration of CM chondrites. *Geochim. Cosmochim. Acta.* **170**, 247–265.

Marrocchi Y., Gounelle M., Blanchard I., Caste F. and Kearsley A. T. (2014) The Paris CM chondrite: Secondary minerals and asteroidal processing. *Meteorit. Planet. Sci.* **49**, 1232–1249.

Matsumoto M., Tsuchiyama A., Nakato A., Matsuno J., Miyake A., Kataoka A., Ito M., Tomioka N., Kodama Y., Uesugi K., Takeuchi A., Nakano T. and Vaccaro E. (2019) Discovery of fossil asteroidal ice in primitive meteorite Acfer 094. *Sci. Adv.* **5**, eaax5078 (10 pp).

Messenger S., Keller L. P., Stadermann F. J., Walker R. M. and Zinner E. (2003) Samples of stars beyond the Solar System: Silicate grains in interplanetary dust. *Science* **300**, 105–108.

Metzler K., Bischoff A. and Stöffler D. (1992) Accretionary dust mantles in CM chondrites: Evidence for solar nebula processes. *Geochim. Cosmochim. Acta* **56**, 2873–2897.

Molster F. J. and Waters L. B. F. M. (2003) The mineralogy of interstellar and circumstellar dust. *In Astromineralogy, ed. Th. Henning, Lecture Notes in Physics* **609**, 121–170.

Nittler L. R., Stroud R. M., Trigo-Rodriguez J. M., De Gregorio B. T., Alexander C. M. O'D., Davidson J., Moyano-Cambero C. E. and Tanbakouei S. (2019) A cometary building block in a primitive asteroidal meteorite. *Nature Astron.* **3**, 659–666.

Newton J., Bischoff A., Arden J. W., Franchi I. A., Geiger T., Greshake A. and Pillinger C. T. (1995) Acfer 094, a uniquely primitive carbonaceous chondrite from the Sahara. *Meteoritics* **30**, 47–56.

Nguyen A. N. and Zinner E. (2004) Discovery of ancient silicate stardust in a meteorite. *Science* **303**, 1496–1499.

Nguyen A. N., Stadermann F. J., Zinner E., Stroud R. M., Alexander C. M. O'D. and Nittler L. R. (2007) Characterization of presolar silicate and oxide grains in primitive carbonaceous chondrites. *Astrophys. J.* **656**, 1223–1240.

Nguyen A. N., Keller L. P. and Messenger S. (2016) Mineralogy of presolar silicate and oxide grains of diverse stellar origins. *Astrophys. J.* **818**, 51 (17 pp).

Noguchi T., Ohashi N., Tsujimoto S., Mitsunari T., Bradley J. P., Nakamura T., Toh S., Stephan T., Iwata N. and Imae N. (2015) Cometary dust in Antarctic ice and snow: Past and present chondritic porous micrometeorites preserved on the Earth's surface. *Earth Planet. Sci. Lett.* **410**, 1–11.

Ohtaki K. K., Patel M. K., Crespillo M. L., Karandikar K. K., Zhang Y., Graeve O. A. and Mecartney M. L. (2018) Improved high temperature radiation damage tolerance in a three-phase ceramic with heterointerfaces. *Scientific Reports* **8**, 1–7.

Ohtaki K. K., Ishii H. A. and Bradley J. P. (2020) Combined focused ion beam-ultramicrotomy method for TEM specimen preparation of porous fine-grained materials. *Microscopy Microanal.* **26**, 120–125.

Palme H., Lodders K. and Jones A. (2014) Solar system abundances of the elements. In Planets, Asteroids, Comets and the Solar System (ed. A. M. Davis), Vol. 2 Treatise on Geochemistry, 2nd Ed. (Exec. Eds. H. D. Holland and K. K. Turekian). Elsevier, Oxford, pp. 15–36

Palme H., Hezel D. C. and Ebel D. S. (2015) The origin of chondrules: Constraints from matrix composition and matrix-chondrule complementarity. *Earth Planet. Sci. Lett.* **411**, 11–19.

Rubin A. E. (2012) Collisional facilitation of aqueous alteration of CM and CV carbonaceous chondrites. *Geochim. Cosmochim. Acta* **90**, 181–194.

Rubin A. E. (2015) An American on Paris: Extent of aqueous alteration of a CM chondrite and the petrography of its refractory and amoeboid olivine inclusions. *Meteorit. Planet. Sci.* **50**, 1595–1612.

Rutherford M. E., Chapman D. J., Derrick J. G., Patten J. R. W., Bland P. A., Rack A., Collins G. S. and Eakins D. E. (2017) Probing the early stages of shock-induced chondritic meteorite formation at the mesoscale. *Scientific Reports* **7**, #45206 (9 pp) and associated Corrigendum **7**, #4691 (1 pp).

Singerling S. A. and Brearley A. J. (2020) Altered primary iron sulfides in CM2 and CR2 carbonaceous chondrites: Insights into parent body processes. *Meteorit. Planet. Sci.* **55**, 496–523.

Stöffler D., Keil K. and Scott E. R. D. (1991) Shock metamorphism of ordinary chondrites. *Geochim. Cosmochim. Acta* **55**, 3845–3867.

Tan H., Verbeeck J., Abakumov A. and Van Tandeloo G. (2012) Oxidation state and chemical shift investigation in transition metal oxides by EELS. *Ultramicroscopy* **116**, 24–33.

Trigo-Rodriguez J. M., Rubin A. E. and Wasson J. T. (2006) Non-nebular origin of dark mantles around chondrules and inclusions in CM chondrites. *Geochim. Cosmochim. Acta* **70**, 1271–1290.

Vacher L. G., Piani L., Rigaudier T., Thomassin D., Glorin G., Piralla M. and Marrocchi Y. (2020) Hydrogen in chondrites: Influence of parent body alteration and atmospheric contamination on primordial components. *Geochim. Cosmochim. Act* **281**, 53–66.

Verdier-Paoletti M. J., Nittler L. R. and Wang J. (2019) First detection of presolar grains in Paris, the most preserved CM chondrite. *Lunar Planet. Sci.* **50**, #2948.

Villalon K. L., Ohtaki K. K., Bradley J. P., Ishii H. A., Davis A. M. and Stephan T. (2021) Search for meteoritic GEMS II: Comparison of inclusions in amorphous silicates from the Paris chondrite and from anhydrous chondritic interplanetary dust particles. *Geochim. Cosmochim. Act* **310**, 346–362.

Vollmer C., Hoppe P., Stadermann F. J., Floss C. and Brenker F. E. (2009a) NanoSIMS analysis and Auger electron spectroscopy of silicate and oxide stardust from the carbonaceous chondrite Acfer 094. *Geochim. Cosmochim. Acta* **73**, 7127–7149.

Vollmer C., Brenker F. E., Hoppe P. and Stroud R. M. (2009b) Direct laboratory analysis of silicate stardust from red giant stars. *Astrophys. J.* **700**, 774–782.

Wark D. A. and Lovering J. F. (1977) Marker events in the early evolution of the solar system: Evidence from rims on Ca-Al-inclusions in carbonaceous chondrites. *Lunar Planet. Sci.* **8**, 95–112.

Wasson J. T. and Rubin A. E. (2010) Matrix and whole-rock fractionations in the Acfer 094 type 3.0 ungrouped carbonaceous chondrite. *Meteorit. Planet. Sci.* **45**, 73–90.

Zanetta P.-M., Leroux H., Le Guillou C., Zanda B. and Hewins R. H. (2021) Nebular thermal processing of accretionary fine-grained rims in the Paris CM chondrite. *Geochim. Cosmochim. Acta* **295**, 135–154.

Zhukovska S., Gail H.-P. and Trieloff M. (2008) Evolution of interstellar dust and stardust in the solar neighborhood. *Astron. Astrophys.* **479**, 453–480.

Associate editor: Eric Quirico